Myeloperoxidase is required for dampening the hydrogen peroxide burst after wounding and for prompt neutrophil migration

Luke Pase[1,2,3], Constantino Carlos Reyes-Aldasoro[4,5], Judith E. Layton[1], Cameron J. Nowell[6], Sony Varma[1,3], Kelly L. Rogers[7], Chris J. Hall[8], Philip S. Crosier[8], Joan K. Heath[9], Stephen A. Renshaw[10], Graham J. Lieschke[1,2,3,11]

1. Cancer and Haematology Division, Walter and Eliza Hall Institute of Medical Research, Parkville, Victoria 3052, Australia.
2. Department of Medical Biology, University of Melbourne, Parkville, Victoria 3010, Australia.
3. Australian Regenerative Medicine Institute, Monash University, Clayton, Victoria 3800, Australia.
4. Cancer Research UK Tumour Microcirculation Group, University of Sheffield, Sheffield S10 2TN, United Kingdom.
5. School of Engineering and Design, University of Sussex, Brighton BN1 9QT, United Kingdom.
6. Centre for Advanced Microscopy, Ludwig Institute for Cancer Research - Parkville, Victoria 3050, Australia
7. Imaging Facility, Walter and Eliza Hall Institute of Medical Research, Parkville, Victoria 3052, Australia.
8. Department of Molecular Medicine and Pathology, School of Medical Sciences, The University of Auckland, Auckland 1142, New Zealand.
9. Colon Molecular and Cell Biology Laboratory, Ludwig Institute for Cancer Research - Parkville, Victoria 3050, Australia.
10. MRC Centre for Developmental and Biomedical Genetics, University of Sheffield, Sheffield S10 2TN, United Kingdom.

11. **Corresponding author:**

Prof. Graham J. Lieschke
Australian Regenerative Medicine Institute
Level 1, Building 75
Monash University, Clayton, Victoria 3800, Australia

Tel: + (61) 3 9902 9720 Fax: + (61) 3 9902 9729
E-mail: Graham.Lieschke@monash.edu

RUNNING TITLE: Requirements for myeloperoxidase after wounding

ABBREVIATIONS

clo, *cloche* mutant; dpf, days post fertilization; *drf, durif* mutant; DsRED2, red fluorescent protein from *Discosoma*; EGFP, enhanced green fluorescent protein; H_20_2, hydrogen peroxide; hpf, hours post fertilization; HyPer, a H_2O_2-sensitive fluorophore; *lyz*, *lysozyme C*; MPO, myeloperoxidase; Mpx/*mpx*, protein and nucleic acid forms respectively of the zebrafish ortholog of myeloperoxidase; trans, transmission light image; WT, wildtype.

WORD/CHARACTER COUNT:

Abstract: 200 words

Text as below: 35,574 characters (not including spaces)

Title page: 1,943

Text: 25,212

Figure legends: 6,934

Acknowledgements etc: 1,485

(Not including Materials and Methods, References, Tables and Supplemental Material)

ABSTRACT

Myeloperoxidase (MPO) is an abundant neutrophil enzyme generating potent antimicrobial chemicals. However, the nature of MPO's essential physiological role has been enigmatic because of the apparent clinical normality of most patients with the common disorder of myeloperoxidase deficiency. We exploit the optical transparency of zebrafish and a new myeloperoxidase-deficient zebrafish mutant (*durif*) that replicates the mammalian MPO-deficiency phenotype to identify two new essential physiological requirements for MPO. Firstly, leukocyte-delivered MPO is a key negative regulator of the burst of tissue-generated hydrogen peroxide (H_2O_2) that occurs following wounding, demonstrated by abnormally sustained H_2O_2 wound concentration profiles in leukocyte-depleted and MPO-deficient animals. Secondly, by *in vivo* leukocyte tracking, we demonstrate that MPO is required for normal neutrophil migration kinetics at the start of acute inflammation. In MPO-deficient animals, the initiation of neutrophil migration towards a wound is delayed, resulting in fewer leukocytes accumulating initially. However, because recruited neutrophils also linger near the wound, accumulated neutrophil numbers later normalize. These data demonstrate that MPO is necessary *in vivo* during early acute inflammation for normal H_2O_2 homeostasis and for normal leukocyte migration. They provide a new basis for understanding beneficial and disadvantageous clinical associations of MPO deficiency suggested by epidemiological and genome-wide association studies.

INTRODUCTION

Leukocyte-derived myeloperoxidase (MPO) is an important component of the inflammatory process. MPO is a major constituent of the primary granules of neutrophil granulocytes, comprising ~5% of their dry weight (Schultz and Kaminker, 1962) and has long been employed as a defining marker of this leukocyte lineage in many species, either by histochemistry, immunohistochemistry, or as a marker in flow cytometry (Klebanoff, 2005; Skubitz, 2009a). MPO is a key enzyme maximizing the antimicrobial potency of the neutrophil respiratory burst. It catalyses the reaction: $Cl^- + H_2O_2 \rightarrow H_2O + OCl^-$ i.e. it consumes hydrogen peroxide (H_2O_2) to generate hypochlorite (OCl^-), a far more potent antimicrobial, in a reaction consuming as much as 72% of the oxygen used in the neutrophil respiratory burst (Thomas et al., 1983). The generation of this potent antimicrobial anion has long been thought to be MPO's primary function (Klebanoff, 2005; Skubitz, 2009a). Recently, however, there has been considerable interest in non-enzymatic roles of myeloperoxidase, for example, its contribution to electrostatic neutrophil attractant forces (Klinke et al., 2011).

The classical picture of neutrophil-mediated, MPO-catalyzed processes relies on the neutrophil oxidative burst to produce the necessary reactive oxygen intermediates. This employs NADPH oxidase (NOX2) to generate superoxide radicals (O_2^-) (Babior et al., 2002) which are rapidly converted to H_2O_2 either spontaneously or enzymatically by superoxide dismutase (SOD) to become available for MPO-mediated catalysis. However, emerging evidence suggests

H_2O_2 and MPO have roles during the inflammatory response other than just the production of oxidizing halogens. It has been proposed that MPO consumption of H_2O_2 generated by the oxidative burst might function predominantly to protect antimicrobial proteases from H_2O_2 within the phagosome (Segal, 2005) and that MPO can modulate vascular nitric oxide levels in a H_2O_2-dependent manner (Eiserich et al., 2002). The role of H_2O_2 during the inflammatory response has been further expanded by the recent findings from *in vivo* studies in zebrafish and flies showing that immediately following wounding, epithelial cells rapidly produce H_2O_2 catalyzed by dual oxidase (Moreira et al., 2010; Niethammer et al., 2009). Importantly, the resultant tissue-scale H_2O_2 gradient serves as an early chemotactic signal to leukocytes (Niethammer et al., 2009).

MPO-deficiency is the most prevalent disorder of human neutrophil function, with an incidence of 1:2000 (Skubitz, 2009b). Many of these have a genetic basis, affecting the processing and assembly of the mature MPO multimer from precursor forms (Hansson et al., 2006). Unexpectedly, given the background outlined above, the clinical consequences of MPO-deficiency are surprisingly subtle, with most MPO-deficient individuals apparently lacking overt infective clinical sequelae. *In vitro*, MPO-deficient neutrophils show delayed bactericidal killing despite normal phagocytosis and a robust respiratory burst (Nauseef, 1988). This does not, however, translate into a pronounced clinical vulnerability to bacterial infection. In contrast, killing of phagocytosed Candida and Aspergillus organisms is impaired, correlating with disseminated fungal infections reported in some MPO-deficient patients (Lehrer and Cline, 1969). Epidemiological studies link increased incidences of inflammatory disease and

severe infections to constitutional MPO-deficiency (Kutter et al., 2000; Lanza, 1998). Acquired MPO-deficiency is common in acute myeloid leukaemia (≈50%), myeloproliferative disease (e.g. 20-60% of chronic myeloid leukaemia) and myelodysplastic syndromes (25%) (Nauseef, 1988), and may contribute to their associated infection vulnerability. Adding to the enigma, the epidemiological associations of MPO-deficiency include not only disease vulnerabilities, but also protection from disease. Genome-wide association studies link the A allele of the -463A/G MPO-promoter polymorphism (which results in lower MPO expression) to a lower risk of some cancers and a lesser risk of early-onset multiple sclerosis (Klebanoff, 2005; van der Veen et al., 2009). While mechanisms for some of these associations have been explored (van der Veen et al., 2009), many remain to be determined.

The myeloperoxidase-deficient knockout mouse replicates the relative normality and subtle infection vulnerability of the human phenotype (reviewed in (van der Veen et al., 2009)). Mpo-deficient mice are vulnerable to some infections (Aratani et al., 1999). Several *in vivo* murine studies have demonstrated that MPO loss results in a reduction of neutrophil accumulation after myocardial, renal or hepatic ischemia and reperfusion (Askari et al., 2003; Klinke et al., 2010; Matthijsen et al., 2007), partly due to impaired neutrophil endothelial adhesion as a result of loss of an MPO-dependent positive electrostatic surface charge on neutrophils (Klinke et al., 2010). However, the relatively minor vulnerability to infection accompanying MPO-deficiency means that the nature of the essential physiological requirements for myeloperoxidase

underpinning the strong evolutionary conservation of its high-level neutrophil expression still remain uncertain.

Zebrafish have proven to be an informative vertebrate disease model with parallel anatomy and physiology particularly suitable for modelling haematological and immunological processes and disorders to mammals (Carradice and Lieschke, 2008; Ellett and Lieschke, 2010). In particular, in zebrafish as in mammals, high-level myeloperoxidase expression is also restricted to neutrophils (Bennett et al., 2001; Lieschke et al., 2001).

In this study, we exploit a new zebrafish mutant (*durif, drf*) that is deficient in myeloperoxidase (Mpx, the zebrafish ortholog of MPO) (Lieschke et al., 2001) to define two new physiological requirements for myeloperoxidase. Our unique, zebrafish myeloperoxidase-deficiency model provides for the simultaneous real-time *in vivo* visualization of tissue-produced H_2O_2 and leukocyte behavior. Leukocyte-delivered myeloperoxidase is demonstrated to be required for dampening wound margin H_2O_2 concentrations. Furthermore, in myeloperoxidase-deficient animals, although the wound H_20_2 gradient is established normally, the initiation of directional neutrophil migration is delayed, resulting in fewer neutrophils initially accumulating at the wound. Later, neutrophil numbers within the wound-zone normalize, because in MPO-deficiency, those neutrophils recruited to the wound also linger there. Collectively, these new observations indicate that myeloperoxidase has essential, non-redundant physiological roles in negatively regulating H_2O_2 signalling and in modulating neutrophil migration *in vivo*.

RESULTS

durif (*drf*) - a myeloperoxidase-deficient zebrafish mutant

drf resulted from the Melbourne Myeloid screen (Hogan et al., 2006), a forward genetic screen of densely ethylnitrosurea-mutated zebrafish genomes designed to collect mutants with recessive defects in myeloid development based on loss of expression of several marker genes including *myeloperoxidase* (*mpx*), the zebrafish ortholog of mammalian Myeloperoxidase (Lieschke et al., 2001). *drf* was recovered as an adult homozygous viable mutant that was neutrophil-replete, but its neutrophils lacked *mpx* transcripts (e.g. by in situ hybridization, Fig. 1A), and lacked Mpx enzymatic activity by two different Mpx-dependent histochemical stains (Fig. 1, B-C). *drf* did not lack any hematopoietic cell type: *drf* retained expression of major hematopoietic lineage specification genes (*tal1/scl*, *spi1/pu.1*, *gata1*, *ikaros*, supplemental Fig. S1, A-L). In particular, *drf* embryos had normal numbers of myeloid cells, evidenced by normal expression of other genes expressed in myeloid cells (*lcp1*, *ncf1*) (Fig. S1, M-P) and normal numbers of cells expressing the Tg(*lyz*:DsRED2) neutrophil-specific transgene (Fig. 1D). Adult *drf* kidney marrow contained neutrophils of normal morphology and ultrastructure, but which lacked Mpx enzymatic activity (Fig. 1, E-F).

The *drf* mutation was linked by 10 cM SSLP-based genome scanning to the chromosome 10 marker z8146, placing it in proximity to the *mpx* locus itself. As a functional genetic test, *drf* was crossed onto the Tg(*mpx*:EGFP) transgenic background (Fig. 1G), in which the EGFP transgene is driven from 127 kb of

BAC-derived *mpx* upstream sequences (Renshaw et al., 2006). In this test, *drf* functioned as a cis-acting rather than trans-regulatory *mpx* mutation because: (1) the Tg(*mpx*:EGFP) transgene was expressed normally in *drf* embryos, excluding the loss of a critical trans-acting *mpx* regulatory factor in *drf*; and (2) *drf* embryos carrying the reporter transgene were still *mpx*-deficient by Sudan Black staining, indicating that there was no rescue by an unsuspected trans-acting *mpx* locus regulatory factor transcribed from the upstream sequences in the BAC-based Tg(*mpx*:EGFP) transgene.

Further mapping positioned *drf* <0.08 cM from RFLP-356k, located ~1.5 kb 3′ of the *mpx* gene (Fig. 1H). Sequence comparisons of WT and *drf* cDNA and genomic DNA and somatic genomic DNA of the ENU-mutated founder male identified an ENU-induced mutation 9 nt upstream of the intron12/exon13 junction (Fig. 1I). This T→A transversion created a new favored splice acceptor site, resulting in a 7 nt insertion in the *drf mpx* transcript. The consequent frameshift generates a predicted stop 3 codons later (Fig. 1I). The resultant truncation eliminates 101 or 232 residues of the two C-terminal variant zebrafish Mpx isoforms, including 41 residues comprising two α-helices of the α-subunit peroxidase domain (pfam03098) (Hansson et al., 2006; Lieschke et al., 2001).

Hence *drf* provides a zebrafish model of congenital myeloperoxidase deficiency with an apparently normal juvenile and adult homozygous viable phenotype that recapitulates the phenotype of both human and murine myeloperoxidase deficiency. We sought to exploit the unique possibilities of this model to test several new hypotheses about the essential role of myeloperoxidase *in vivo*.

The initial decline in wound H_2O_2 concentrations requires leukocyte-delivered myeloperoxidase

Previous studies using a larval zebrafish inflammation model that exploited unique *in vivo* imaging possibilities in zebrafish had demonstrated that hydrogen peroxide (H_2O_2) was the earliest leukocyte chemoattractant after wounding (Niethammer et al., 2009). In these studies, concurrence of leukocyte arrival and the ensuing initial decline in wound H_2O_2 concentrations was described, but a causal relationship was not investigated. Since myeloperoxidase catalyzes a reaction consuming H_2O_2, we hypothesized that leukocyte-delivered myeloperoxidase was a key negative regulator of the initial burst of tissue-produced H_2O_2.

Firstly, this hypothesis requires that the decline in H_2O_2 levels after wounding be leukocyte-dependent. To determine if the concurrence of leukocyte arrival and a decline in wound H_2O_2 concentration was coincidental or causally-related, H_2O_2 concentration dynamics were monitored in leukocyte-depleted embryos. To monitor leukocyte numbers, transgenic zebrafish with fluorophore-marked leukocytes were used (Hall et al., 2007; Renshaw et al., 2006), and to monitor H_2O_2 concentrations, the highly-selective, genetically-encoded, H_2O_2-sensitive fluorophore HyPer was used (Belousov et al., 2006). Wildtype (WT) and leukocyte-depleted embryos (Fig. 2A) had similar acute increases in wound margin H_2O_2 concentrations, indicating that initial H_2O_2 production is not leukocyte-dependent (Fig. 2B). However, in contrast to WT, in which H_2O_2

concentrations peaked at 28±4 (mean±SD) min after wounding and then declined, in leukocyte-depleted embryos, the wound margin H_20_2 concentration was sustained at near-peak levels for ≥90 min (Fig. 2B). Furthermore, in WT embryos, the H_20_2 response was limited to the wound vicinity, but in leukocyte-depleted embryos, H_20_2 concentrations progressively increased in the trunk distant to the wound (Fig. 2C). These differences were not artefacts of morpholino-loaded embryos, since they were replicated in the mutant *cloche*, which has a genetically-based deficiency of all hematopoietic cell types including leukocytes (Stainier et al., 1995) (Fig. 1, B-C; supplemental Movie M1). Overall, H_20_2 concentration profiles were statistically significantly different between each of these leukocyte-depleted scenarios and WT (Fig. 2B, ii-iii). Hence, leukocytes are required for a normal decline of wound margin H_20_2 concentrations after the initial burst of H_20_2 production.

Secondly, this hypothesis also requires that neutrophil myeloperoxidase and H_20_2 functionally interact at the wound margin. To experimentally confirm this, a histochemical test was performed (Fig. 3). In the standard histochemical myeloperoxidase stain, production of a brown precipitate in neutrophils is dependent on the Mpx enzymatic activity in the cells and the H_20_2 supplied in the staining solution, as demonstrated by the absence of staining in Mpx-deficient *drf* embryos stained with standard solutions (Figs 1B, 3C) and in uninjured WT embryos when exogenous H_20_2 was not added (Fig. 3E). By performing the stain without exogenous H_20_2, we tested whether sufficient H_20_2 was produced endogenously after wounding for Mpx to generate the indicator precipitate. Without exogenous H_20_2, scattered cells stained at the wound, but

there was no staining in cells away from the wound in the caudal hematopoietic tissue (CHT) of WT embryos (Fig. 3B), nor was there staining in wounded *drf* embryos (Fig. 3D). Taken together, this indicates that sufficient H_20_2 was produced endogenously at the wound margin for Mpx within WT neutrophils to catalyze local deposition of the indicator precipitate.

Thirdly, to functionally test if myeloperoxidase was an essential neutrophil-delivered negative regulator of wound margin H_20_2 concentration, H_20_2 concentrations after wounding were compared between WT and the new mutant *drf*. Since *drf* was genetically Mpx-deficient but neutrophil-replete, it permitted the functional requirement for neutrophil-delivered Mpx to be tested. WT and *drf* embryos exhibited similar rapid acute increases in wound margin H_20_2 concentrations, indicating that initial H_20_2 production is not Mpx-dependent. In scans selected for equivalent numbers of DsRED2-expressing neutrophils arriving (Fig. S2A), wound margin H_20_2 concentrations remained elevated at peak levels for up to ≥90 min after wounding in *drf* embryos (Fig. 4, A-B; supplemental Movie M2) at the time H_20_2 concentrations were declining in comparable WT scans. This essentially replicated the scenario in leukocyte-depleted *spi1/csf3r* morphants (Fig. 2, B-C). Overall, H_20_2 concentration profiles were statistically significantly different between *drf* and WT (Fig. 4Aii). Similar statistically-significant genotype differences were observed on a line scanning confocal microscope: *drf* showed persistently high H_2O_2 concentrations at the wound zone up to 3 h after amputation (Fig. S2, B-C; supplemental Movie M3).

This defect in *drf* was not due to an increased susceptibility to phototoxicity or a *drf*-dependent alteration in HyPer emission performance, as non-wounded *drf* and WT embryos maintained uniformly low HyPer/H_20_2 levels and showed no difference (Fig. 4Ai).

A particularly instructive scan, in which only a single *lyz*-DsRED2-marked neutrophil arrived, provided evidence that even a single neutrophil could bring sufficient Mpx to reduce the local H_20_2 concentration (Fig. S3; supplemental Movie M4). In this example, the HyPer-monitored H_20_2 concentration declined regionally as a *lyz*-DsRED2-marked neutrophil moved through the dorsal part of the tail wound (such cells have >90% likelihood of being a strongly *mpx*-expressing neutrophil, see Table S3), but movement of three leukocytes not expressing the *lyz*:DsRED2 reporter through the ventral wound zone did not locally suppress the H_20_2 concentration (these cells are highly likely to be macrophages which do not express the *lyz*:DsRED2 transgene (Ellett et al., 2011; Meijer et al., 2008)).

Collectively, these three lines of evidence strongly support the hypothesis that neutrophil-delivered *Mpx* is required for a normal rate of decline from the peak H_20_2 concentrations after wounding.

Myeloperoxidase-deficient neutrophils linger at the wound edge

Current evidence demonstrates that both myeloperoxidase and H_20_2 play a positive role in leukocyte recruitment to a site of injury (Klinke et al., 2010;

Niethammer et al., 2009). The combination of the zebrafish wound model permitting imaging of each neutrophil attracted to the wounded tailfin and Mpx-deficient *drf* embryos provided a unique opportunity to assess the functional consequence on overall leukocyte migratory behavior of the loss of one of these positive elements, myeloperoxidase, in the face of sustained high levels of the other positive neutrophil chemoattractant, wound margin H_20_2 concentrations.

8 h timelapse videomicrographs of wounded WT and *drf* embryos on the Tg(*mpx*:EGFP) background were collected and an extensive range of parameters that might reflect altered neutrophil behaviors were defined. Sensitivity analyses were undertaken where components of the parameter definitions were arbitrary, such as what represented a directional movement, or what constituted the "wound zone". (Table S2).

Interestingly, no striking differences in velocity or directionality parameters were noted. However, these data pointed to a difference in behaviour of neutrophils leaving the wound zone. The "move away from wound ratio", a parameter defined to reflect the tendency of moving neutrophils to remain within the wound zone, showed a robust difference between WT and *drf* (Fig. 5A) that was most marked, and attained statistical significance, when the wound was defined more narrowly e.g. a zone of <200 μm (Fig. 5B). The lower "move away from wound ratio" in *drf* indicated a tendency for mobile neutrophils to remain there for longer, particularly within a more narrowly-defined wound zone corresponding to the region of highest H_20_2 concentration (compare Fig. 2C

with Fig. 4B). There was no difference in the number of static neutrophils between *drf* and WT larvae.

Without myeloperoxidase, initiation of neutrophil migration to the wound is delayed

The initial phase of the inflammatory response, during which WT and *drf* embryos exhibited similar rapid acute increases in wound margin H_20_2 concentration, was also scrutinized to determine the direct requirement of Mpx for neutrophil motion towards the wound. Manual scoring of the time at which neutrophils initiated directional movement towards the wound demonstrated significantly delayed initiations in *drf*, which was more marked at greater distances from the wound (Fig. 6Ai-ii). This was independent of whether neutrophils were marked by *mpx*:EGFP or *lyz*:DsRED2 transgenes (Fig. 6Ai-ii) and was corroborated by a custom algorithm-based analysis of the same data using the computed parameter "time to initiation of directed movement" (Fig. 6Bi-ii). This extends previous observations (Klinke et al., 2011) and suggests that the reduced recruitment of MPO-deficient neutrophils results from a delayed response to the chemotactic stimulus.

The overall cumulative impact of the altered leukocyte migration kinetics was evaluated in 3 independent experiments determining neutrophil numbers within a narrowly-defined wound zone at timepoints up to 36 h after wounding (Fig. 6C; Fig. S4A-B). Compared to those in WT, neutrophils in *drf* showed a slower rate of rise to peak number and significantly lower peak neutrophil

numbers at 4 and/or 6 h after wounding. *drf* neutrophils also dwelt longer within the wound zone. This was demonstrated by the normalised decrease in numbers between peak and 24 h timepoints after wounding, which was significantly lower in *drf* than WT embryos (Fig. 6D), independently confirming the observation above based on the algorithm-derived "move away from wound ratio". For timepoints ≥24 h after wounding, wound zone neutrophil numbers were similar between genotypes.

DISCUSSION

This new zebrafish model of myeloperoxidase deficiency shows significant phenotypic concordance with the prevalent human disorder and also with the corresponding murine model. In all three species, high-level myeloperoxidase expression is specific to neutrophils, and MPO-deficiency is genetically recessive with adult homozygous viability, apparently normal survival, and normal numbers of morphologically normal neutrophils throughout life.

Although MPO deficiency is the commonest human neutrophil disorder, its impact on health and disease has been controversial. While many MPO-deficient individuals appear phenotypically normal, some associative studies suggest vulnerability to various inflammatory and infective disorders, whereas other epidemiological studies have identified protective disease associations (Klebanoff, 2005; Kutter et al., 2000; Lehrer et al., 1969; Rudolph et al., 2010; van der Veen et al., 2009). Our observations indicate that studies seeking to understand the mechanisms of such disease associations should consider altered H_2O_2 clearance and/or perturbed leukocyte migration dynamics as potential contributing factors, rather than focusing exclusively on hypochlorous acid production and its contribution to microbial killing and/or tissue damage.

This study demonstrated a new process by which neutrophils directly modulate tissue-generated H_2O_2, their earliest known chemoattractant, by its rapid down-regulation. Technical possibilities uniquely offered by the new zebrafish *mpx*-deficient mutant enabled the demonstration *in vivo* that arriving neutrophils

dampen wound-induced H_2O_2 levels by an *mpx*-dependent mechanism. Since sufficient H_20_2 is produced locally for leukocyte Mpx activity to be histochemically detectable near the wound, this is most likely directly dependent on Mpx enzymatic activity (which consumes H_20_2), rather than on some other indirect mechanism. However, it is likely that Mpx is not the only factor involved; anti-oxidants in adjacent cells must be involved also, as is demonstrated by the complete dampening of H_2O_2 at very small fin injuries, before neutrophil arrival and in *drf* (data not shown). Once neutrophils arrive, other enzymes they deliver could be involved in the decomposition of H_20_2 (e.g. catalase) and production of H_20_2 (NADPH oxidase and superoxide dismutase). However, the similar H_2O_2 concentration profiles in leukocyte-depleted and *mpx*-deficient scenarios suggest that dual oxidase-dependent H_2O_2 production exceeds the combined sequestering capacity of endogenous antioxidants and other neutrophil delivered antioxidants and enzymes. It also indicates that leukocyte-generated H_2O_2 makes a minor contribution to overall wound zone H_2O_2 levels within the first 90 min of wounding.

The inferred wound margin H_2O_2 concentration of 0.5-50 μM (Belousov et al., 2006; Niethammer et al., 2009) is appropriate for Mpx to generate reactive halides (Klebanoff, 2005). This provides a process that immediately converts the weakly microbicidal H_2O_2 into much more potent antimicrobial halides at the right place (wound edge) at the right time (on neutrophils arrival). It also provides for generation of potent antimicrobials without activation of the neutrophil oxidative burst, and indicates that dual oxidase-dependent supply of H_2O_2 to MPO is more important than previously recognized (Klebanoff, 2005).

However, the neutrophil oxidative burst is important for other aspects of the inflammatory response, given the more severe defects in patients with NAPDH oxidase subunit defects than is seen with MPO deficiency (Kuhns et al., 2010).

Although H_20_2 signalling to leukocytes was initially studied in zebrafish wounds, evidence points to its wide general relevance. In zebrafish, tumor cell sensing by leukocytes has recently been shown to involve H_20_2 signalling (Feng et al., 2010) and wound produced H_20_2 promotes peripheral sensory axon regeneration following injury (Rieger and Sagasti, 2011). Wound-related H_20_2 signalling has now been demonstrated in flies (Moreira et al., 2010). Mammalian/murine neutrophils display a direct chemotactic response to H_20_2 *in vitro* at relevant concentrations (Klyubin et al., 1996). In an *in vitro* scratch-wound model using a human keratinocyte cell line, H_20_2 promoted keratinocyte migration re-epithelialization (Loo et al., 2011), demonstrating a functional link between H_20_2 and cell migration in another human cell type important in wounding. The high degree of parallelism between zebrafish and mammalian hematologic development, hematologic cell function, cellular innate immunity and inflammatory processes (for reviews, see (Carradice and Lieschke, 2008; Ellett and Lieschke, 2010)) underpins the value of zebrafish as a surrogate model in these systems (Bolker, 2009). However, despite some recent advances in *in vivo* imaging of mammalian leukocyte behaviors (e.g. (McDonald et al., 2010)), confirmation of the findings of our studies in mammalian systems *in vivo* will require significant *in vivo* imaging advances.

This study also demonstrated that normal neutrophil behavior during inflammation has several requirements for Mpx. Firstly, in the chronic absence of Mpx, the initiation of neutrophil migration is delayed. H_2O_2 is currently the earliest-acting known neutrophil chemoattractant and since the initial rate of rise in tissue-generated H_2O_2 concentrations after wounding follows the same temporal profile in WT and *drf* embryos, the altered neutrophil behavior in *drf* points to a role for Mpx influencing neutrophil motility that is upstream of H_2O_2-directed chemotaxis. This may be an H_2O_2/Mpx-dependent process involving other substrates important for neutrophil migration (e.g. nitrogen species including nitric oxide (Eiserich et al., 2002)), or an H_2O_2-independent Mpx effect such as the loss of the Mpx electrostatic forces shown recently to be important for neutrophil migration *in vitro* (Klinke et al., 2010). Alternatively, Mpx deficiency may alter the intrinsic H_2O_2 threshold of neutrophils towards requiring a higher H_2O_2 concentration before migration starts. Distinguishing between these possibilities will require both technical advances and novel reagents.

Secondly, Mpx deficiency resulted in reduced peak accumulation of neutrophils at the site of injury, a result concordant with MPO null mice (Askari et al., 2003; Klinke et al., 2010; Matthijsen et al., 2007). This suggests that during the period of inflammation when there is a maintained high H_2O_2 concentration at the wound margin, loss of an Mpx-dependent function (e.g. endothelial adhesion aided by Mpx electrostatic forces (Klinke et al., 2010)) is epistatic to H_2O_2-driven neutrophil recruitment to a site of injury. However, interestingly, once an Mpx-deficient neutrophil arrives at the wound zone (<200 μm), the area where there

is the greatest maintenance of high H_2O_2 concentrations, its departure is also then postponed.

In conclusion, it has long been accepted that the primary function of MPO is to generate reactive halide species to kill microorganisms (Klebanoff, 2005), although other roles are being recognized (Eiserich et al., 2002; Klinke et al., 2010; Lau et al., 2005). These studies show that it is also a key regulator of inflammatory H_20_2 gradients and of leukocyte migration *in vivo*. The superior tools and methods for visualising H_20_2 gradients and leukocyte tracking *in vivo* in zebrafish will underpin ongoing contributions from this model to the understanding of H_20_2 signalling gradients and leukocyte migration in inflammation.

MATERIALS AND METHODS

Zebrafish

Zebrafish strains were: AB*, *cloche* (*clo*^{m39}) (Stainier et al., 1995), Tg(*mpx*:EGFP)^{i114} (Renshaw et al., 2006), Tg(*lyz*:DsRED2)^{nz50} (Hall et al., 2007), Tg(*mpeg1*:GAL4)X(UAS:Kaede) (Ellett et al., 2011) and *durif* (*drf*^{gl8}). Fish were housed in the Ludwig Institute for Cancer Research Aquarium using standard husbandry practices. Experiments were conducted at 28°C. From 12 hpf, embryos were held in 0.003% 1-phenyl-2-thiourea (Sigma-Aldrich) in egg water (0.06 g/L salt (Red Sea, Sydney, Australia)). Animal experiments followed the NHMRC "Australian code of practice for the care and use of animals for scientific purposes" and were approved by the Animal Ethics Committees of the Ludwig Institute for Cancer Research (AEC Approval IDs 17/01 and 18/01) and the Walter and Eliza Hall Institute (AEC Approval IDs 2005.045, 2007.012 and 2009.027). Zebrafish gene, protein and mutant naming follows the recommended conventions at http://zfin.org/zf_info/nomen.html; specifically for zebrafish myeloperoxidase, "*mpx*" indicates the gene or transcript, and "Mpx" indicates the protein.

Leukocyte depletion

1-2 cell Tg(*lyz*:DsRED2) embryos were microinjected with 1 nl of *spi1* (Rhodes et al., 2005) and *csf3r* (Liongue et al., 2009) morpholino antisense oligonucleotides (500 and 250 μM respectively) (GeneTools). 3 dpf embryos with <20 DsRED2-expressing cells were selected for experiments.

Gene expression analysis

Whole mount in situ hybridisation (WISH) used standard techniques, with *in vitro* transcribed digoxigenin-labelled antisense riboprobes (Carradice and Lieschke, 2008) and 4-nitroblue tetrazolium/5-bromo-4-chloro-3-indolyl phosphate for detection.

Mapping and positional cloning

drf was identified in the Melbourne myeloid screen (Hogan et al., 2006). 10 cM genome scanning used a standard SSLP marker set. Table S1 lists SSLP and RFLP markers used. Most mapping pairs were a heterozygous female and homozygous *drf* male. 48 hpf offspring were phenotyped by WISH *mpx* expression. Recombinants were identified in phenotypically *drf* embryos by gain of heterozygosity and in phenotypically WT embryos by gain of homozygosity.

Sequencing the *mpx* locus and transcript

mpx exons, exon/intron boundaries and ~2 kb of promoter were sequenced from genomic DNA from a homozygous *drf* adult, a WT AB* embryo and the somatic DNA of the founder mutagenized male. *mpx* mRNA transcripts were isolated from 3 dpf embryos using Trizol (Life Technologies) and RNeasy kit (QIAGEN). cDNA was generated using standard reverse transcription conditions. Intron 12 splicing was assessed by sequencing PCR product generated with primers mpx_cDNA_F/R (all primer sequences in Table S1).

Myeloperoxidase enzymatic assays

For Sudan Black staining, embryos were fixed (4% paraformaldehyde (PFA) / PBS, 2 h, room temperature) and PFA removed by rinsing (5 min, PBS, X3). Samples were submerged in 500 µl Sudan Black Staining Solution (Sigma-Aldrich) for 20 min and destained with 70% ethanol (several rinses initially, then soaked for 30 min periods until adequate clarity was reached).

For whole mount *mpx* histochemistry, embryos were fixed (3.7% formaldehyde/90% ethanol, 1 min) and washed in water (1 min, X3). Embryos were placed in plastic 6-well plates (Costar), excess water removed and freshly made staining solution added: TRIZMAL™ 6.3 Dilute Buffer containing 1 vial Peroxidase Indicator Reagent (1-part p-phenylenediamine dihydrochloride and 2-parts catechol) (Sigma-Aldrich) and 0.12% H_2O_2. Embryos were incubated for 15 min in the dark at room temperature and washed 3X in 4% PFA/PBS for 10 min. For experiments omitting exogenous H_20_2, incubation was for 30 min.

For *mpx* histochemistry on adult cells, cytocentrifuged posterior kidney marrow cells were stained as described (Lieschke et al., 2001).

Electron microscopy

Adult posterior kidneys were fixed, processed and imaged in the Department of Pathology, University of Melbourne, as previously described (Lieschke et al., 2001).

Imaging of wounded embryos for HyPer-based H_20_2 monitoring

HyPer (Evrogen, Moscow, Russia) cDNA was subcloned into pCS2+. *In vitro* transcription following *Not*1 linearization used mMESSAGE mMACHINE (Ambion). 1-2-cell embryos were microinjected with 1-2 nL HyPer mRNA (250 μg/mL). 3 dpf HyPer-mRNA-injected embryos containing *lyz*:DsRED2 positive cells along the caudal tail were wounded by tail fin amputation (Pase et al., 2011). For some experiments, embryos were preselected prior to wounding for adequate neutrophil numbers in the distal tail (the experiments of Figs 2, 4, 5, 6A-B, supplemental Fig. S2). There was no preselection for leukocyte migration studies (the experiments of Fig. 6,C-D; Fig. S4). A Nikon Ti-E microscope with a 20x PlanFluor NA/0.5 objective (Nikon), was used to image every 30 s for 90 min, maintaining samples at 28°C with an incubator (Clearstate Solutions, Australia). Acquisition used a SPOT Pursuit Slider CCD camera (Diagnostic Instruments) and MetaMorph software (v7.7.0, Molecular Devices). A Prior ProScan II (Prior, UK) motorized stage was used for multipoint imaging. Four images were captured at each time point: a brightfield/DIC image, a violet excitation/green emission image ($HyPer_{420}$) using a custom filter cube (ex420/20, 505LP, em535/20), a blue excitation/green emission image ($HyPer_{480}$) using a Nikon B-2E/C filter cube (ex480/15, 505LP, em535/20) and a green excitation/red emission image (for *lyz*:DsRED2 neutrophils) using a Nikon G-2E/C filter (ex540/25, 565LP, em620/30).

In some experiments, 512 x 512 pixel images were captured every 30 s for up to 3 h using a fully motorised inverted line-scanning confocal microscope equipped with an environmental chamber maintained at 28°C (LSM 5 Live, Zeiss, Germany). A single optical section was acquired using a Plan-Apochromat

20x/0.8 NA objective with 0.5X Zoom and wide aperture (pinhole - 100 μm). For the calculation of HyPer excitation ratios ($YFP_{500/420}$), YFP emission was recorded consecutively through a BP495-555 filter following fluorescence excitation with a 488 and 405 nm laser. Neutrophil (*lyz*:DsRED2) detection was performed with a BP575-615 + LP655 filter/ NFT565 and 561 nm laser excitation. Corresponding brightfield images were captured.

Image analysis

Ratio analysis of HyPer images used custom-written journals in MetaMorph (v7.7.0. Molecular Devices, USA) as comprehensively described (Pase et al., 2011). In brief, the $HyPer_{420}$ and $HyPer_{480}$ excitation images were median filtered, background was subtracted, the tail area extracted using a threshold. A HyPer ratio image ($HyPer_{480}/HyPer_{420}$) was generated using image calculator in ImageJ (v1.43).

HyPer images acquired on the line scanning confocal microscope were analysed as above, but with an additional background correction for differences in the horizontal vignetting between the 405 and 488 laser paths. These HyPer ratio images were divided by a 512 x 512 pixel background ratio image generated from the 512 median column ratio values ($HyPer_{488}/HyPer_{405}$) of a scan of a uniform blue fluorescent slide (Chroma), reiterated across the 512 rows.

To graph changes in $[H_2O_2]$ at the wound margin, the median HyPer ratio ($HyPer_{480}/HyPer_{420}$ or $HyPer_{488}/HyPer_{405}$) was taken within a manually-defined ~50 μm wound edge zone using ImageJ. The “Percentage of maximum hydrogen

peroxide level" (Fig. S2) was calculated as $(HyPer_{488}/HyPer_{405})^{wound\ zone}/(HyPer_{488}/HyPer_{405})^{distal\ region}$ for each time point as a percentage of the maximum value observed. "Distal region" was defined as a 10^4 μm^2 region of the trunk, >400 μm from the wound edge. If required, movement of the embryo tail was corrected using ImageJ.

Computational leukocyte tracking and path analysis

Analyses of 4-dimensionsal leukocyte imaging datasets were performed in MATLAB (C). The segmentation algorithm performed intensity-based segmentation with a hysteresis double threshold, with high and low thresholds determined based on Otsu's algorithm (Otsu, 1979). Volume elements (voxels) below and above the lower threshold were classified as background and neutrophils respectively. Intermediate-level voxels were classified as cells if in contact with voxels above the high threshold, or as background otherwise. Tracking was performed with a keyhole model of movement (Reyes-Aldasoro et al., 2008) where cell movement is predicted to follow one of two possibilities: either completely random around the current position of the cell, or oriented following the same orientation and velocity as the previous jump. These options are translated into two regions of probability: a circle and a wedge, together resembling a keyhole. Several post-processing tasks were performed: initial nodes were validated with a backward linking of nodes, tracks for which neutrophils disappear for one frame were joined, small tracks were discarded, and collisions between neutrophils were detected and cells split to be re-tracked. Finally, manual validation of the tracks removed outliers and joined tracks that the algorithm could not link.

From these tracks, a series of measurements related to cell behavior was examined, as tabulated in Table S2 and exemplified in Figs 5 and 6B. The "time to initiation of directed movement" emerged as an important parameter. To estimate the instant at which a neutrophil began migrating in a directed way towards a wound, each movement between consecutive frames was projected (as a vector decomposition) towards a line perpendicular to the wound. The components of the movement towards and parallel to the wound were considered the *oriented distance* and *lateral distance* respectively and used to calculate *oriented* and *lateral velocities*. To fulfil the condition of sustained movement, the oriented velocity of the subsequent 40 frames (or until the neutrophil track ended or entered the wound) was calculated. To be considered active, tracks were required to have at least 15 frames remaining after initiation. For each track, the activation point was the moment when both oriented and sustained velocities exceeded a predefined threshold of 4 pixels/frame.

Statistical analyses

Descriptive and analytical statistics were prepared in Prism 5 (Version 5.0a) (GraphPad Software Inc). Unless otherwise stated, p-values are 2-tailed and derive from unpaired t-tests for parametric data and Mann-Whitney tests for non-parametric or non-normally distributed data.

For the data in Figs 2B, 4A, and Fig. S2B**,** the hypotheses were tested using a natural permutation test. The null hypothesis was that there was no difference between the population mean curve for the wildtype and experimental groups.

The test statistic was the absolute difference D between these two sample mean curves. The significance of the observed difference D was computed by comparing it to the distribution of D-values for all possible random splits of the combined set of animals into two datasets with sizes equal to the original sizes, one set designated "wildtype" and the other as "experimental". Since the total number of such random splits is not large, they could all be enumerated. The p-value assigned under the null hypothesis was the proportion of random splits giving a D-value larger than or equal to the observed difference D. In practice, this was calculated by dividing the rank of the observed D in the list of all possible D-values by the total number of such splits.

ONLINE SUPPLEMENTAL MATERIAL

Fig S1 (related to Fig. 1) shows the expression of a range of hematopoietic genes in the *myeloperoxidase*-deficient zebrafish mutant *durif*. Fig. S2 (related to Figs 2 and 4) documents the comparability of neutrophil arrival data in the individual animals contributing to wildtype and *durif* datasets used for H_2O_2 concentration profile comparisons, and presents additional data collected on an alternate microscope showing that abnormally high injury-induced H_2O_2 concentrations are maintained for up to 3 h after injury in *myeloperoxidase*-deficient larvae. Fig. S3 provides data showing that a single neutrophil is sufficient to reduce the local wound zone H_2O_2 concentration. Fig. S4 (related to Fig. 6C) presents additional data and analyses showing that neutrophil numbers at a wound edge show consistent differences between wildtype and *durif* embryos. Movie M1 (related to Fig. 2) provides a real time comparison of H_2O_2 concentrations, displayed by HyPer ratiometric data heat maps, in representative wildtype and leukocyte-depleted embryos for 90 min after wounding. Movie M2 (related to Fig. 4) provides a real time comparison of H_2O_2 concentrations, displayed by HyPer ratiometric data heat maps, in representative wildtype and *myeloperoxidase*-deficient *durif* embryos for 90 min after wounding. Movie M3 (related to Fig. S2B) provides a longer (3 h) real time comparison of H_2O_2 concentrations, displayed by HyPer ratiometric data heat maps, in representative wildtype and *myeloperoxidase*-deficient *durif* embryos after wounding, collected on an alternate microscope. Movie M4 (related to Fig. S3) shows the complete scan demonstrating the changes in wound margin H_2O_2 concentration as a single *lyz*:DsRED2-marked neutrophil migrates to and within the wound zone.

Table S1 tabulates the oligonucleotides used in this study. Table S2 tabulates fifteen computationally-derived custom parameters used to assess neutrophil migration following wounding, and provides a detailed footnote about the methodology used to derive them. Table S3 documents the degree of overlap of transgene expression in Tg(*lyz*:DsRED2)/(*mpx*:EGFP) and Tg(*lyz*:DsRED2)/(*mpeg1*:GAL4)/(10xUAS:Kaede) compound transgenic zebrafish.

ACKNOWLEDGEMENTS

We thank: J. Hayman (technical assistance); M. Greer, K. Turner and P. Chamberlain (aquarium care); F. Ellett, W. Alexander, N. Nicola, N. Rosenthal, B. Croker (discussions); T. Speed and M. Olshansky (statistical advice); S. Jane, D. Curtis and RMH-BMRL (support); Centre for Advanced Microscopy (Ludwig Institute for Cancer Research) and the Australian Cancer Research Foundation Centre for Therapeutic Target Discovery (microscopy). GL received grant support from NIH (R01 HL079545), NHMRC (234708, 461208, 637394) and ARC (DP0346823). LP was supported by an Australian Postgraduate Award and WEHI Edith Moffatt Scholarship. WEHI receives infrastructure support from the Commonwealth NHMRC Independent Research Institutes Infrastructure Support Scheme (361646) and a Victorian State Government Operational Infrastructure Support Scheme grant. The Australian Regenerative Medicine Institute is supported by grants from the State Government of Victoria and the Australian Government. The funders had no role in study design, data collection and analysis, decision to publish, or preparation of the manuscript. The authors have no conflicting financial interests.

AUTHOR CONTRIBUTIONS

LP performed most of the research. JEL generated *drf* and commenced mapping. CJN and KLR assisted with imaging and image analysis. SV provided technical assistance. CCRA and SAR provided Tg(*mpx:*EGFP) fish and assisted with neutrophil tracking analyses. CJH and PSC provided Tg(*lyz*:DsRED2) fish and data regarding reporter transgene overlap. JKH contributed to mutant mapping

and discussion. GJL and LP conceived the research and wrote the manuscript. All authors reviewed the manuscript and interpreted and discussed data.

REFERENCES

Aratani, Y., H. Koyama, S. Nyui, K. Suzuki, F. Kura, and N. Maeda. 1999. Severe impairment in early host defense against Candida albicans in mice deficient in myeloperoxidase. *Infect Immun* 67:1828-1836.

Askari, A.T., M.L. Brennan, X. Zhou, J. Drinko, A. Morehead, J.D. Thomas, E.J. Topol, S.L. Hazen, and M.S. Penn. 2003. Myeloperoxidase and plasminogen activator inhibitor 1 play a central role in ventricular remodeling after myocardial infarction. *J Exp Med* 197:615-624.

Babior, B.M., J.D. Lambeth, and W. Nauseef. 2002. The neutrophil NADPH oxidase. *Arch Biochem Biophys* 397:342-344.

Belousov, V.V., A.F. Fradkov, K.A. Lukyanov, D.B. Staroverov, K.S. Shakhbazov, A.V. Terskikh, and S. Lukyanov. 2006. Genetically encoded fluorescent indicator for intracellular hydrogen peroxide. *Nat Methods* 3:281-286.

Bennett, C.M., J.P. Kanki, J. Rhodes, T.X. Liu, B.H. Paw, M.W. Kieran, D.M. Langenau, A. Delahaye-Brown, L.I. Zon, M.D. Fleming, and A.T. Look. 2001. Myelopoiesis in the zebrafish, Danio rerio. *Blood* 98:643-651.

Bolker, J.A. 2009. Exemplary and surrogate models: two modes of representation in biology. *Perspect Biol Med* 52:485-499.

Carradice, D., and G.J. Lieschke. 2008. Zebrafish in hematology: sushi or science? *Blood* 111:3331-3342.

Eiserich, J.P., S. Baldus, M.L. Brennan, W. Ma, C. Zhang, A. Tousson, L. Castro, A.J. Lusis, W.M. Nauseef, C.R. White, and B.A. Freeman. 2002. Myeloperoxidase, a leukocyte-derived vascular NO oxidase. *Science* 296:2391-2394.

Ellett, F., and G.J. Lieschke. 2010. Zebrafish as a model for vertebrate hematopoiesis. *Curr Opin Pharmacol* 10:563-570.

Ellett, F., L. Pase, J.W. Hayman, A. Andrianopoulos, and G.J. Lieschke. 2011. mpeg1 promoter transgenes direct macrophage-lineage expression in zebrafish. *Blood* 117:e49-56.

Feng, Y., C. Santoriello, M. Mione, A. Hurlstone, and P. Martin. 2010. Live imaging of innate immune cell sensing of transformed cells in zebrafish larvae: parallels between tumor initiation and wound inflammation. *PLoS Biol* 8:e1000562.

Hall, C., M.V. Flores, T. Storm, K. Crosier, and P. Crosier. 2007. The zebrafish lysozyme C promoter drives myeloid-specific expression in transgenic fish. *BMC Dev Biol* 7:42.

Hansson, M., I. Olsson, and W.M. Nauseef. 2006. Biosynthesis, processing, and sorting of human myeloperoxidase. *Arch Biochem Biophys* 445:214-224.

Hogan, B.M., J.E. Layton, U.J. Pyati, S.L. Nutt, J.W. Hayman, S. Varma, J.K. Heath, D. Kimelman, and G.J. Lieschke. 2006. Specification of the primitive myeloid precursor pool requires signaling through Alk8 in zebrafish. *Curr Biol* 16:506-511.

Klebanoff, S.J. 2005. Myeloperoxidase: friend and foe. *J Leukoc Biol* 77:598-625.

Klinke, A., C. Nussbaum, L. Kubala, K. Friedrichs, T.K. Rudolph, V. Rudolph, H.J. Paust, C. Schroder, D. Benten, D. Lau, K. Szocs, P.G. Furtmuller, P. Heeringa, K. Sydow, H.J. Duchstein, H. Ehmke, U. Schumacher, T. Meinertz, M. Sperandio, and S. Baldus. 2010. Myeloperoxidase attracts neutrophils by physical forces. *Blood*

Klyubin, I.V., K.M. Kirpichnikova, and I.A. Gamaley. 1996. Hydrogen peroxide-induced chemotaxis of mouse peritoneal neutrophils. *Eur J Cell Biol* 70:347-351.

Kuhns, D.B., W.G. Alvord, T. Heller, J.J. Feld, K.M. Pike, B.E. Marciano, G. Uzel, S.S. DeRavin, D.A. Priel, B.P. Soule, K.A. Zarember, H.L. Malech, S.M. Holland, and J.I. Gallin. 2010. Residual NADPH oxidase and survival in chronic granulomatous disease. *N Engl J Med* 363:2600-2610.

Kutter, D., P. Devaquet, G. Vanderstocken, J.M. Paulus, V. Marchal, and A. Gothot. 2000. Consequences of total and subtotal myeloperoxidase deficiency: risk or benefit ? *Acta Haematol* 104:10-15.

Lanza, F. 1998. Clinical manifestation of myeloperoxidase deficiency. *J Mol Med* 76:676-681.

Lau, D., H. Mollnau, J.P. Eiserich, B.A. Freeman, A. Daiber, U.M. Gehling, J. Brummer, V. Rudolph, T. Munzel, T. Heitzer, T. Meinertz, and S. Baldus. 2005. Myeloperoxidase mediates neutrophil activation by association with CD11b/CD18 integrins. *Proc Natl Acad Sci U S A* 102:431-436.

Lehrer, R.I., and M.J. Cline. 1969. Leukocyte myeloperoxidase deficiency and disseminated candidiasis: the role of myeloperoxidase in resistance to Candida infection. *J Clin Invest* 48:1478-1488.

Lehrer, R.I., J. Hanifin, and M.J. Cline. 1969. Defective bactericidal activity in myeloperoxidase-deficient human neutrophils. *Nature* 223:78-79.

Lieschke, G.J., A.C. Oates, M.O. Crowhurst, A.C. Ward, and J.E. Layton. 2001. Morphologic and functional characterization of granulocytes and macrophages in embryonic and adult zebrafish. *Blood* 98:3087-3096.

Liongue, C., C.J. Hall, B.A. O'Connell, P. Crosier, and A.C. Ward. 2009. Zebrafish granulocyte colony-stimulating factor receptor signaling promotes myelopoiesis and myeloid cell migration. *Blood* 113:2535-2546.

Loo, A.E., R. Ho, and B. Halliwell. 2011. Mechanism of hydrogen peroxide-induced keratinocyte migration in a scratch-wound model. *Free Radic Biol Med* 51:884-892.

Matthijsen, R.A., D. Huugen, N.T. Hoebers, B. de Vries, C.J. Peutz-Kootstra, Y. Aratani, M.R. Daha, J.W. Tervaert, W.A. Buurman, and P. Heeringa. 2007. Myeloperoxidase is critically involved in the induction of organ damage after renal ischemia reperfusion. *Am J Pathol* 171:1743-1752.

McDonald, B., K. Pittman, G.B. Menezes, S.A. Hirota, I. Slaba, C.C. Waterhouse, P.L. Beck, D.A. Muruve, and P. Kubes. 2010. Intravascular danger signals guide neutrophils to sites of sterile inflammation. *Science* 330:362-366.

Meijer, A.H., A.M. van der Sar, C. Cunha, G.E. Lamers, M.A. Laplante, H. Kikuta, W. Bitter, T.S. Becker, and H.P. Spaink. 2008. Identification and real-time imaging of a myc-expressing neutrophil population involved in inflammation and mycobacterial granuloma formation in zebrafish. *Dev Comp Immunol* 32:36-49.

Moreira, S., B. Stramer, I. Evans, W. Wood, and P. Martin. 2010. Prioritization of competing damage and developmental signals by migrating macrophages in the Drosophila embryo. *Curr Biol* 20:464-470.

Nauseef, W.M. 1988. Myeloperoxidase deficiency. *Hematol Oncol Clin North Am* 2:135-158.

Niethammer, P., C. Grabher, A.T. Look, and T.J. Mitchison. 2009. A tissue-scale gradient of hydrogen peroxide mediates rapid wound detection in zebrafish. *Nature* 459:996-999.

Otsu, N. 1979. Threshold Selection Method from Gray-Level Histograms. *IEEE T Syst Man Cyb* 9:62-66.

Pase, L., C.J. Nowell, and G.J. Lieschke. 2011. In vivo real time visualization of leukocytes and intracellular hydrogen peroxide levels during a zebrafish acute inflammation assay. *Methods Enzymol* In Press:

Renshaw, S.A., C.A. Loynes, D.M. Trushell, S. Elworthy, P.W. Ingham, and M.K. Whyte. 2006. A transgenic zebrafish model of neutrophilic inflammation. *Blood* 108:3976-3978.

Reyes-Aldasoro, C.C., S. Akerman, and G.M. Tozer. 2008. Measuring the velocity of fluorescently labelled red blood cells with a keyhole tracking algorithm. *J Microsc* 229:162-173.

Rhodes, J., A. Hagen, K. Hsu, M. Deng, T.X. Liu, A.T. Look, and J.P. Kanki. 2005. Interplay of pu.1 and gata1 determines myelo-erythroid progenitor cell fate in zebrafish. *Developmental Cell* 8:97-108.

Rieger, S., and A. Sagasti. 2011. Hydrogen peroxide promotes injury-induced peripheral sensory axon regeneration in the zebrafish skin. *PLoS Biol* 9:e1000621.

Rudolph, V., R.P. Andrie, T.K. Rudolph, K. Friedrichs, A. Klinke, B. Hirsch-Hoffmann, A.P. Schwoerer, D. Lau, X. Fu, K. Klingel, K. Sydow, M. Didie, A. Seniuk, E.C. von Leitner, K. Szoecs, J.W. Schrickel, H. Treede, U. Wenzel, T. Lewalter, G. Nickenig, W.H. Zimmermann, T. Meinertz, R.H. Boger, H. Reichenspurner, B.A. Freeman, T. Eschenhagen, H. Ehmke, S.L. Hazen, S.

Willems, and S. Baldus. 2010. Myeloperoxidase acts as a profibrotic mediator of atrial fibrillation. *Nat Med* 16:470-474.

Schultz, J., and K. Kaminker. 1962. Myeloperoxidase of the leucocyte of normal human blood. I. Content and localization. *Arch Biochem Biophys* 96:465-467.

Segal, A.W. 2005. How neutrophils kill microbes. *Annu Rev Immunol* 23:197-223.

Skubitz, K.M. 2009a. Neutrophilic Leukocytes. In Wintrobe's Clinical Hematology. J.P. Greer, J. Foerster, G.M. Rodgers, F. Paraskevas, B. Glader, D.A. Arber, and R.T. Means Jnr, editors. Wolters Kluwer / Lippincott Williams and Wilkins, Philadelphia. 170-213.

Skubitz, K.M. 2009b. Qualitative Disorders of Leukocytes. In Wintrobe's Clinical Hematology. J.P. Greer, J. Foerster, G.M. Rodgers, F. Paraskevas, B. Glader, D.A. Arber, and R.T. Means Jnr, editors. Wolters Kluwer / Lippincott Williams and Wilkins, Philadelphia. 1549-1564.

Stainier, D.Y., B.M. Weinstein, H.W. Detrich, 3rd, L.I. Zon, and M.C. Fishman. 1995. Cloche, an early acting zebrafish gene, is required by both the endothelial and hematopoietic lineages. *Development* 121:3141-3150.

Thomas, E.L., M.B. Grisham, and M.M. Jefferson. 1983. Myeloperoxidase-dependent effect of amines on functions of isolated neutrophils. *J Clin Invest* 72:441-454.

van der Veen, B.S., M.P. de Winther, and P. Heeringa. 2009. Myeloperoxidase: molecular mechanisms of action and their relevance to human health and disease. *Antioxid Redox Signal* 11:2899-2937.

FIGURE LEGENDS

Figure 1. *Myeloperoxidase* (*mpx*) deficiency in the zebrafish mutant *durif* (*drf*).

For these analyses, *drf* embryos were generated from homozygote incrossing.

A. *mpx* expression by whole mount in situ hybridization (WISH) in wildtype (WT) and *drf* embryos.

B. Loss of cells carrying Mpx activity in *drf* demonstrated by loss of Mpx-dependent histochemical staining.

C. Loss of cells carrying Mpx activity in *drf* demonstrated by loss of Mpx-dependent stable sudanophilia.

D. Normal Tg(*lyz*:DsRED2) expression in *drf* neutrophils.

E. Cytospun adult kidney hematopoietic cells, stained for Mpx by diaminobenzidine (DAB) histochemistry with May-Grunwald/Giemsa counterstain. WT but not *drf* neutrophils show Mpx staining (black triangles). Both genotypes have Mpx-negative eosinophils (black arrow) and weak staining of erythrocytes due to the pseudoperoxidase Lepehne reaction (open triangles), providing negative and positive staining technique controls. Scale bar, 10 μm.

F. Ultrastructure of adult WT and *drf* neutrophils, showing normal primary granules. Scale bars: left, 2 μm; right, 100 nm.

G. *drf* Tg(*mpx*:EGFP) hemizygotes contain normal numbers of cells expressing the Tg(*mpx*:EGFP) transgene. Histogram shows mean±SE (WT n=16, *drf* n=15).

H. Positional cloning placed *drf* on chromosome 10 within 0.08 cM of the RFLP-356k located ~1.5 kb 3′ from the *mpx* gene.

I. Schematic of the *mpx* locus (black, exon; white, UTR; based on GenBank BC068379.1). Left sequencing chromatograms of cDNA shows the exon 11/12 junction: a 7 nt insertion in *drf* introduces a premature stop codon (*). Right sequencing chromatograms of genomic DNA show the *drf* mutation (red arrow), a T→A transversion 9 nt 5′ of the intron 12/exon 13 junction.

Figure 2. Leukocytes are required for the initial decline in wound margin H_2O_2 concentrations.

A. 3.5 dpf Tg(*lyz*:DsRED2) embryos with >90% reduction in neutrophil numbers in *spi1*/*csf3r* morphants.

B. (i) Mean HyPer ratios reflecting the wound zone H_2O_2 concentration profile of wildtype (WT, injured and uninjured), *cloche* mutant (*clo*) and *spi1*/*csf3r* morphant embryos. Wound zone is the tailfin area within 50 μm of the wound, or 10^4 μm^2 of midline caudal tailfin in non-wounded embryos. Note the significantly sustained, elevated HyPer ratio/H_2O_2-concentration in leukocyte-deficient *clo* and *spi1*/*csf3r* morphants. Insets (ii) and (iii) show the individual median HyPer data and p-values (natural permutation test). Data replication (n embryos/independent days/scans): injured WT 5/2/4; *spi1/csf3r* morphants 4/2/3; *clo* 6/3/5; uninjured WT 5/1/5.

C. Representative HyPer heat maps depicting H_2O_2 concentrations across the wounded tail fin. Overlayed transmission (Trans) and

DsRED images demonstrate the proximity of Tg(*lyz*:DsRED) neutrophils to the wound margin. Note the single DsRED positive cell in the *spi1*/*csf3r* morphant (white arrow head). *clo* did not carry the *lyz*:DsRED transgene. Scale bar (applies to all panels, 200 μm). Stills are from supplemental Movie M1.

Figure 3. Endogenous levels of H_2O_2 interact enzymatically with myeloperoxidase at the wound margin.

Histochemical staining for Mpx activity in wildtype (WT) and *durif* (*drf*) embryos in the presence/absence of added H_2O_2 and/or wounding. For each reaction condition A-E, 3 panels are shown: (i) overview (ii) details of cells in the caudal hematopoietic tissue (iii) wound zone. Stained cells (white arrows) indicate Mpx-dependent catalysis of p-phenylenediamine and catechol. When H_2O_2 is supplied as a reagent, cells stain throughout the embryo (A), but without supplemented H_2O_2, cells stain only at the wound margin (B). C-E are controls: (C,D) *drf* controls show that staining is *mpx*-dependent regardless of the H_2O_2 source; (E) WT uninjured control showing that detecting staining of wound-proximate cells is injury-dependent. x/y indicates: (number of embryos with at least one positive cell with the region)/(number of embryos scored).

Figure 4. Myeloperoxidase is required for the initial decline in wound margin H_2O_2 concentrations.

A. (i) Mean HyPer ratios reflecting the wound zone H_20_2 concentration data for injured and uninjured *drf* embryos. Note the sustained, elevated HyPer ratio/H_20_2-concentration in *mpx*-deficient *drf* mutants. Wound zone definitions as for Fig. 2B. These *drf* data are directly comparable with data of Fig. 2B, and shares its WT control group. Inset (ii) show the individual median HyPer data and p-values compared to WT (natural permutation test). Data replication (n embryos/independent days/scans): injured *drf* 6/5/6; uninjured *drf* 4/1/4.

B. Representative HyPer heat maps depicting H_20_2 concentrations across the wounded tail fin of a *mpx*-deficient *drf* embryo. Overlaid transmission (Trans) and DsRED images demonstrate the proximity of neutrophils to the wound margin. Scale bar, 200 μm. Stills are from Supplemental Movie M2 at directly comparable timepoints to the WT control data in Fig. 2C.

Figure 5. Myeloperoxidase-deficient neutrophils linger at the wound margin.

A. The "move away from wound ratio", a computed parameter reflecting the tendency of moving neutrophils to move away from wound zone, plotted as a function of arbitrary wound zone dimension and track length. With narrowing of the arbitrary wound zone dimension, this parameter diverges for WT (blue) and *drf* (red) neutrophils. Data are from multiple neutrophil tracks from 8 WT and

8 *drf* embryos, analysed by custom computational approaches as detailed in Methods and Table S2.

B. Displays the corresponding p-values, the flat burgundy mat indicating p=0.05. p-values for this parameter are <0.05 for the combination of longer minimum track durations (>150 min) and smaller arbitrary wound zones (<150 μm).

Figure 6. Delayed initiation of neutrophil migration towards a wound in myeloperoxidase deficiency.

A. Manually-scored "neutrophil movement initiation time", the time-to-initiation of strongly directional movement towards wound zone.
(i) *mpx*:EGFP-marked neutrophils, pooled from 5 WT and 4 *drf* embryos. r^2 for lines of best fit: WT, 0.71; *drf*, 0.56; gradients are significantly different (p=0.030).
(ii) *lyz*:DsRED2-marked neutrophils, pooled from 14 WT and 10 *drf* embryos. r^2 for lines of best fit: WT, 0.50; *drf*, 0.62; gradients are significantly different (p=0.024).

B. Dataset of A(i), re-analysed by a custom-designed algorithm applied to tracking data, determining a computed parameter, the "time to initiation of directed movement".
(i) Example of neutrophil tracks in a WT embryo. Colored lines tracks individual neutrophils; horizontal dimensions map location within the tail (imaged in the horizontal projection); vertical axis depicts time after wounding. Circles indicate the point designated by the algorithm as the "time of initiation of directed movement".

(ii) Analysis outcome for the "time to initiation of directed movement", corroborating the manually-scored data of panel A(i). r^2 for lines of best fit: WT, 0.24; *drf*, 0.25; the difference in elevation is significantly different ($p<0.0001$).

C. Cumulative number of neutrophils in the wound zone (within 80-100 μm of wound margin) over 24 h period post-wounding, for a larger wound involving the notochord (insert is schematic diagram of wound type). Consistent with slower migration initiation demonstrated above, neutrophil accumulation at the wound zone is slower in *drf* than WT (1.7±0.2 vs 3.2±0.5 neutrophils/h, $p=0.002$; further details in supplemental Fig. S4, C), resulting in significantly different wound margin neutrophil numbers between genotypes 4 h after wounding (**, $p=0.0034$). Consistent with their greater lingering in *drf*, wound zone neutrophil numbers are equivalent ≥12 h after wounding. Data are mean±SE (n=12 for each genotype). Inset is diagram of injury: C, caudal fin; N, notochord; V, vasculature; W, wound; blue shading indicates 80-100 μm wound zone.

D. Plot of the % change in neutrophil numbers from peak after wounding numbers to 24 h after wounding (peak in WT, 6 h; in *drf,* 8 h). Data are pooled from 31 WT and 30 *drf* embryos from experiments represented in panel C, and supplemental Fig. S4, A-B. Two-tailed Mann-Whitney test.

Figure 1

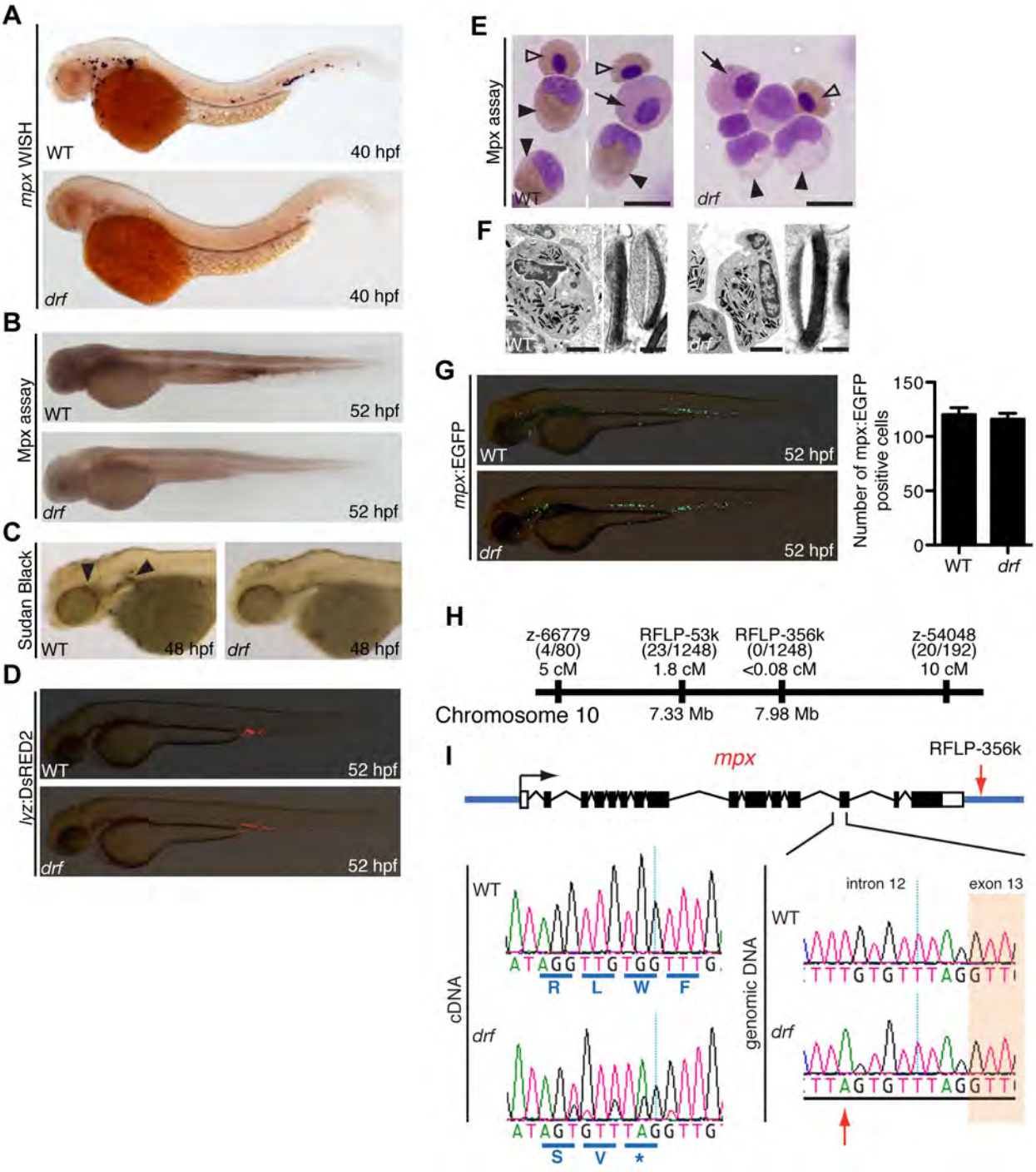
A
mpx WISH
WT
40 hpf
drf
40 hpf
B
Mpx assay
WT
52 hpf
drf
52 hpf
C
Sudan Black
WT
48 hpf
drf
48 hpf
D
lyz:DsRED2
WT
52 hpf
drf
52 hpf
E
Mpx assay
WT
drf
F
WT
drf
G
mpx:EGFP
WT
52 hpf
drf
52 hpf
Number of mpx:EGFP positive cells
150
100
50
0
WT
drf
H
z-66779
(4/80)
5 cM
RFLP-53k
(23/1248)
1.8 cM
RFLP-356k
(0/1248)
<0.08 cM
z-54048
(20/192)
10 cM
Chromosome 10
7.33 Mb
7.98 Mb
I
mpx
RFLP-356k
cDNA
WT
ATAGGTTGTGGTTTG
R L W F
drf
ATAGTGTTTAGGTTG
S V *
genomic DNA
intron 12
exon 13
WT
TTTGTGTTTAGGTT
drf
TTAGTGTTTAGGTT

Figure 2

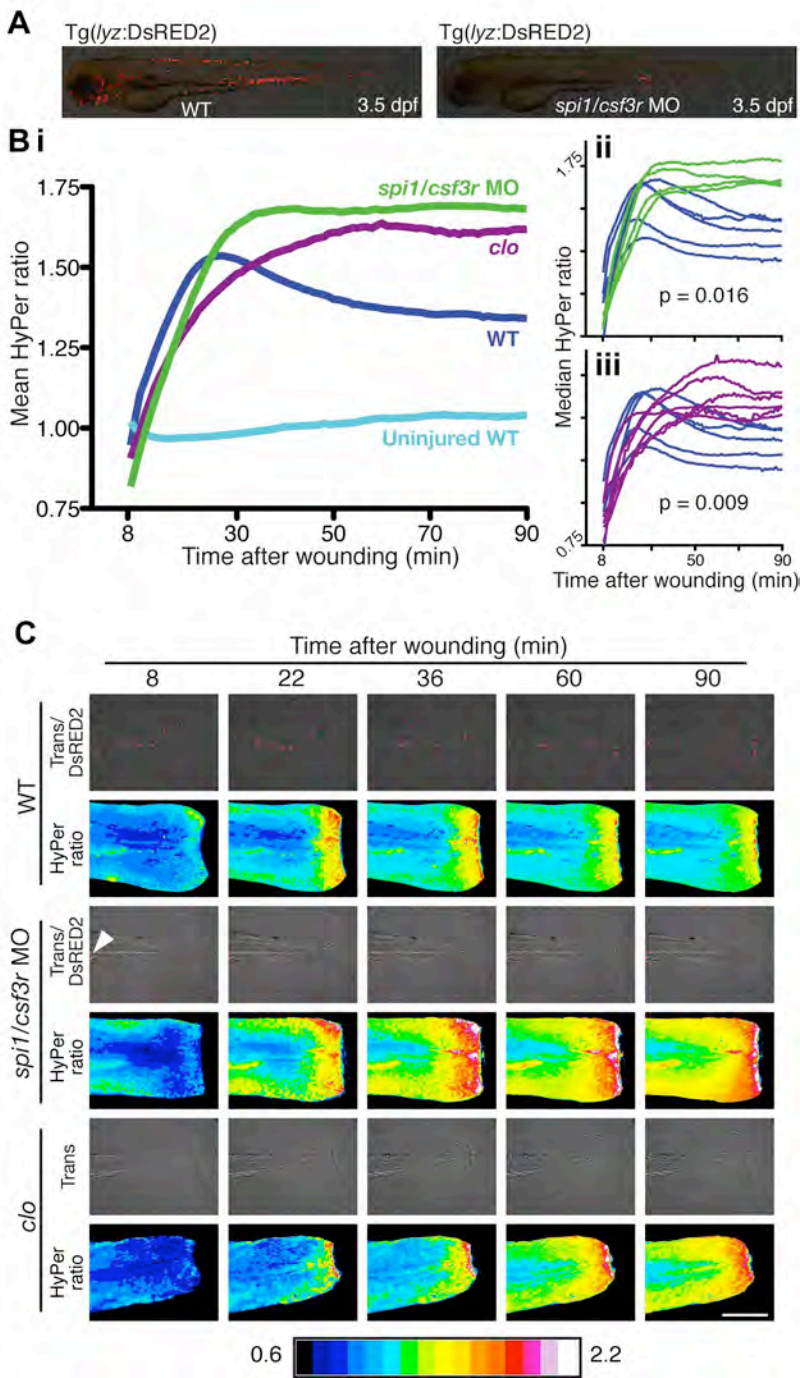
A
Tg(lyz:DsRED2)
WT
3.5 dpf
Tg(lyz:DsRED2)
spi1/csf3r MO
3.5 dpf
B i
Mean HyPer ratio
1.75
1.50
1.25
1.00
0.75
spi1/csf3r MO
clo
WT
Uninjured WT
8
30
50
70
90
Time after wounding (min)
ii
Median HyPer ratio
1.75
p = 0.016
iii
p = 0.009
0.75
8
50
90
Time after wounding (min)
C
Time after wounding (min)
8
22
36
60
90
WT
Trans/ DsRED2
HyPer ratio
spi1/csf3r MO
Trans/ DsRED2
HyPer ratio
clo
Trans
HyPer ratio
0.6
2.2

Figure 3

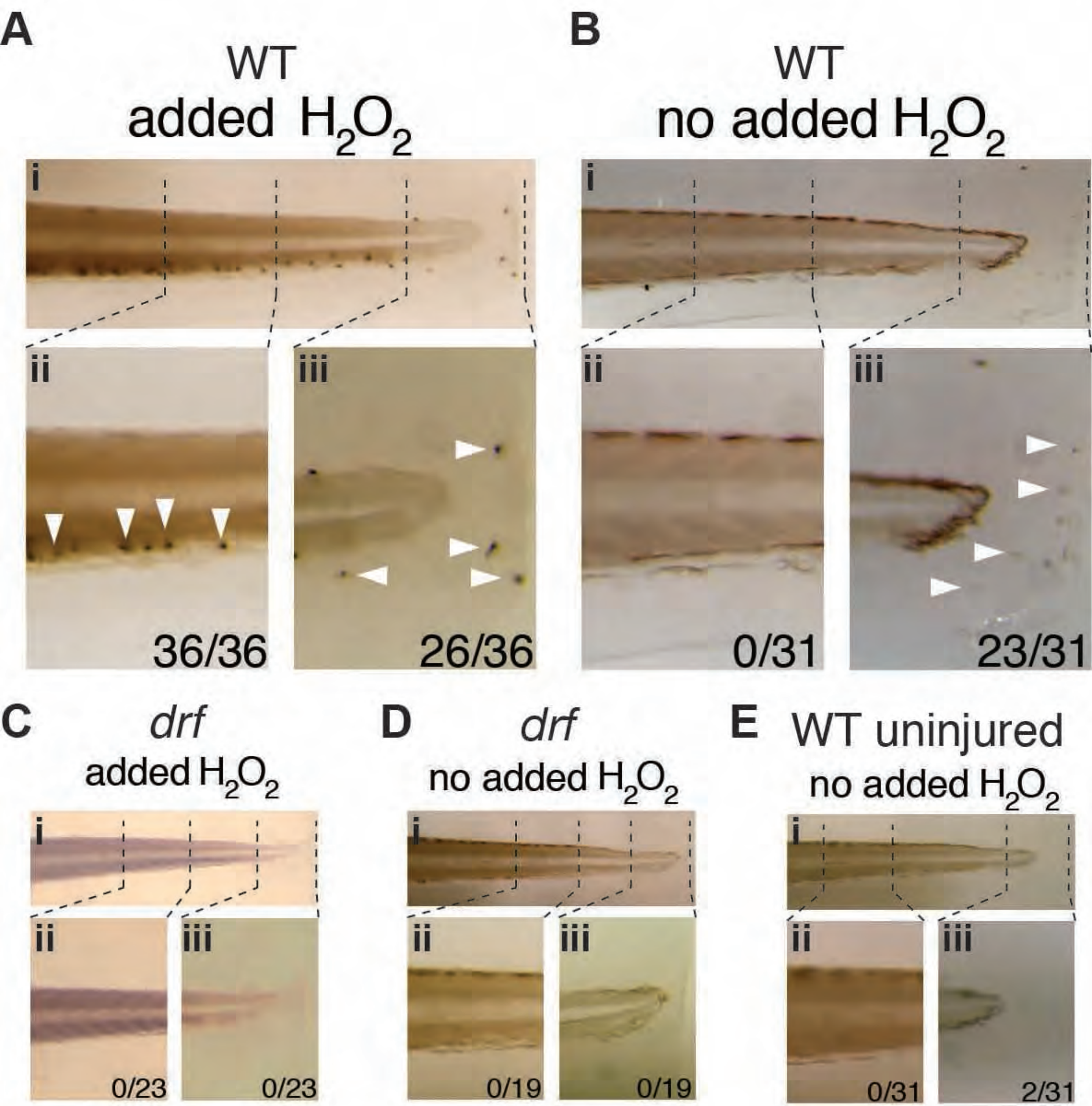
A
WT
added H_2O_2
i
ii
iii
36/36
26/36
B
WT
no added H_2O_2
i
ii
iii
0/31
23/31
C
drf
added H_2O_2
i
ii
iii
0/23
0/23
D
drf
no added H_2O_2
i
ii
iii
0/19
0/19
E
WT uninjured
no added H_2O_2
i
ii
iii
0/31
2/31

Figure 4

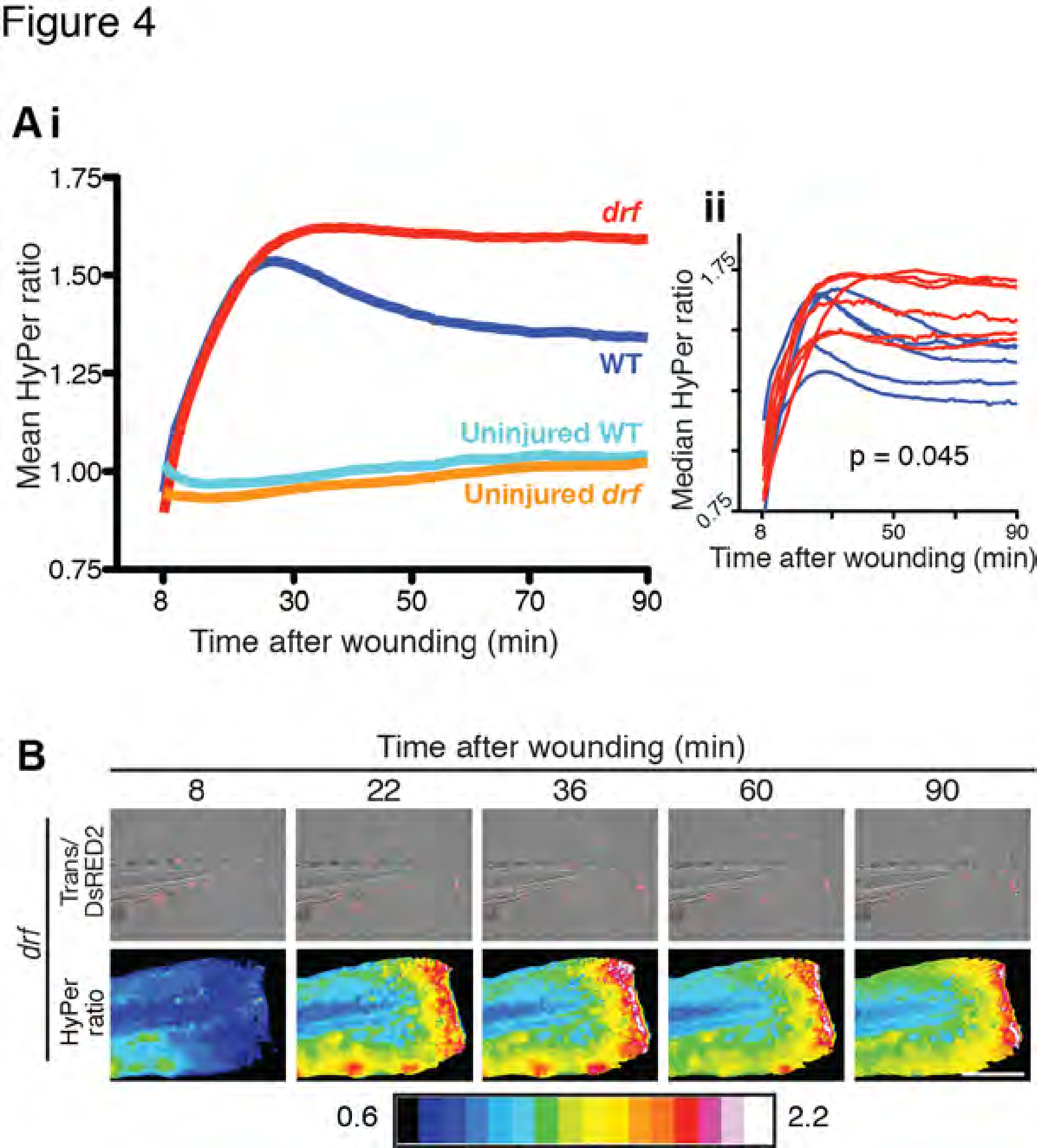
Ai
1.75
1.50
1.25
1.00
0.75
Mean HyPer ratio
drf
WT
Uninjured WT
Uninjured drf
8
30
50
70
90
Time after wounding (min)
ii
Median HyPer ratio
1.75
0.75
p = 0.045
8
50
90
Time after wounding (min)
B
Time after wounding (min)
8
22
36
60
90
drf
Trans/ DsRED2
HyPer ratio
0.6
2.2

Figure 5

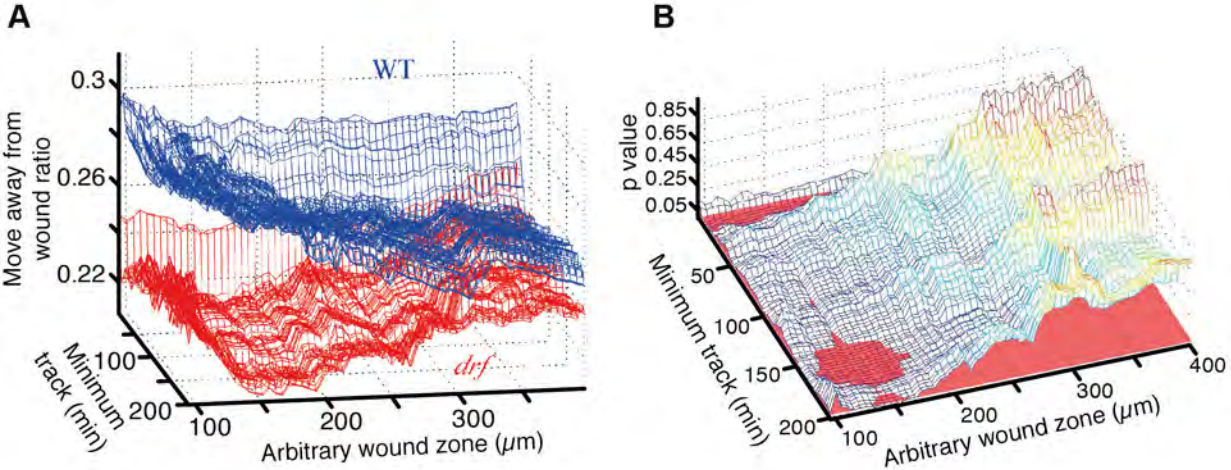
A
WT
drf
0.3
0.26
0.22
Move away from wound ratio
Minimum track (min)
100
200
100
200
300
Arbitrary wound zone (μm)
B
p value
0.85
0.65
0.45
0.25
0.05
Minimum track (min)
50
100
150
200
100
200
300
400
Arbitrary wound zone (μm)

Figure 6

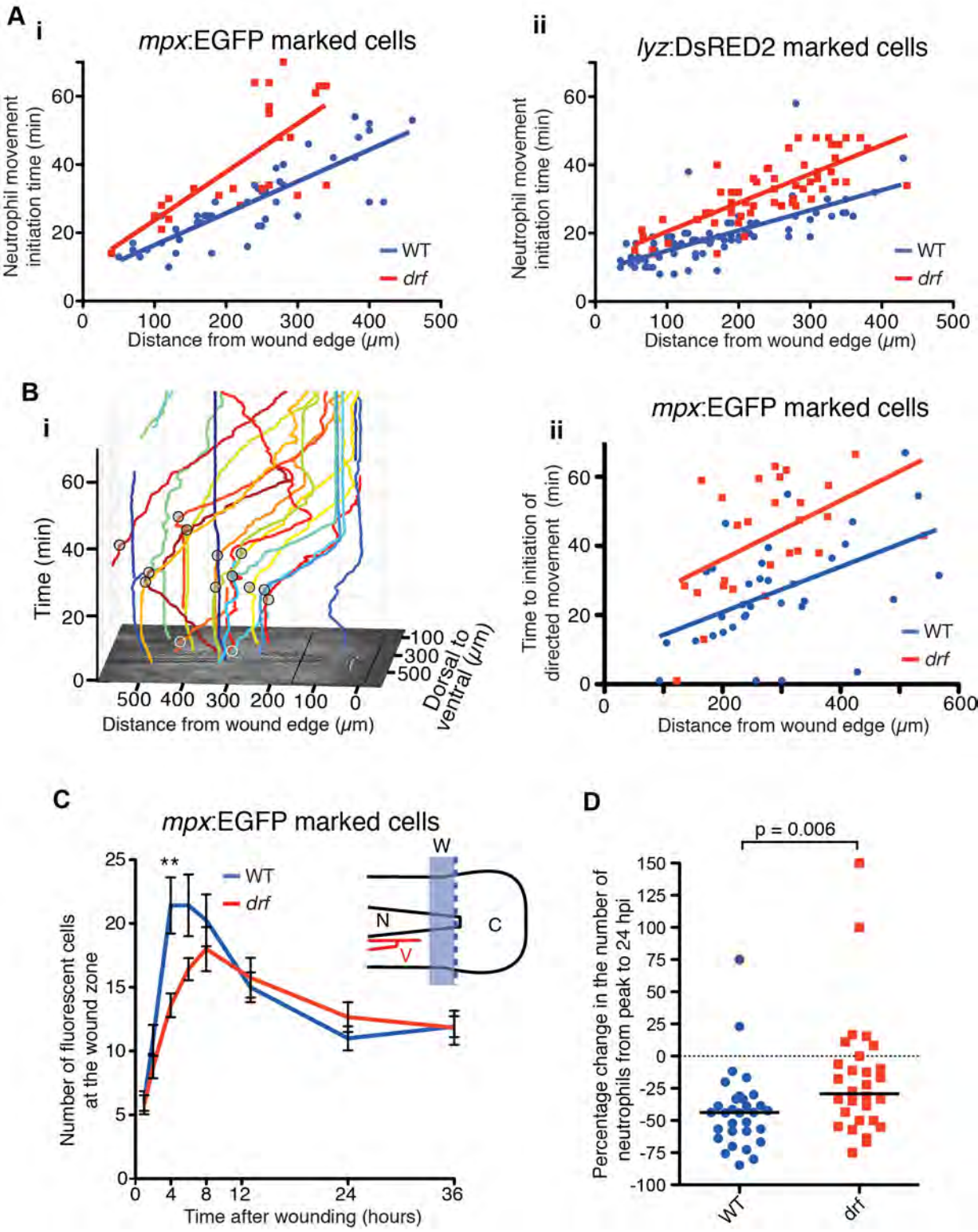
A
i
mpx:EGFP marked cells
Neutrophil movement initiation time (min)
Distance from wound edge (μm)
WT
drf
ii
lyz:DsRED2 marked cells
Neutrophil movement initiation time (min)
Distance from wound edge (μm)
WT
drf
B
i
Time (min)
Distance from wound edge (μm)
Dorsal to ventral (μm)
ii
mpx:EGFP marked cells
Time to initiation of directed movement (min)
Distance from wound edge (μm)
WT
drf
C
mpx:EGFP marked cells
Number of fluorescent cells at the wound zone
Time after wounding (hours)
WT
drf
**
W
N
V
C
D
p = 0.006
Percentage change in the number of neutrophils from peak to 24 hpi
WT
drf

Table S1. Oligonucleotides used in this study.

Name	Sequence 5´ ⇒ 3´	Purpose and comments
z8146_F	AGCGGAGATGATGACTTGGT	SSLPs that aided the positional cloning of *durif*
z8146_R	TCCGCCTCTAGAGAGACTGC	
Z66779_F	TCAGCATTCCAGGTCTGATTT	
z66779_R	GGGACAGGAACAGCCATACA	
z54048_F	GCACCACATTTTAAGCAGCA	
z54048_R	TTTGGGAGCAGCTTTTCTGT	
RFLP-53k_F	TGAACAGTGATCGGGAACAG	Amplify a HaeIII RFLP that aided the positional cloning of *durif*
RFLP-53k_R	TTCACCCATAATGTGCGTTG	
RFLP-356_F	TGGCACGCATAGTACAGCAT	Amplify an AseI RFLP that aided the positional cloning of *durif*
RFLP-356_R	TGCAGCACCAAAGAAAACAG	
mpx_LP-1_F	CCAATGATGCTCAGCAGACT	Amplify and sequence the *mpx* promoter, exons and intron/exon junctions
mpx_LP-2_R	AAAGACCCAAAATCACCCGT	
mpx_LP-3_F	AATGCCATGTGTAAGTGTGAAA	
mpx_LP-4_R	TGAGGGGTCTGGTCCTACAA	
mpx_LP-5_F	TCAAGACGAGCTTCAAACCA	
mpx_LP-6_R	GACTGACCGAAATTGGGAAG	
mpx_LP-7_F	GGGTTGACCACGATCTGACT	
mpx_LP-8_R	ACATACCCGCAATGAAGCAAG	
mpx_LP-9_F	CACAATTTAGGTTTGACAAATGC	
mpx_LP-10_R	GGTTGGAAAGAAGATAATGGACC	
mpx_LP-11_F	CTGCGAGGCTTCTTGCTACT	
mpx_LP-12_R	ACCTGGAAGGTCAAACACCA	
mpx_LP-13_F	TTGGTTTAAGGGGATTTGCTT	
mpx_LP-14_R	GTAAAGCAGAACCAGCCCAA	

mpx_LP-15_F	GAGACTTGTTGCAGCATACC	
mpx_LP-16_R	TTGAATGGAGACACTTGTGG	
mpx_LP-17_F	ACTGGTTCTGGACTTGAAGC	
mpx_LP-18_R	GAACAACAGCCAACAAGTGG	
mpx_LP-19_F	GGAAACGGTTCTTTCAAGTTC	
mpx_LP-20_R	TCCTGGCATCTTAGTCAGAG	
mpx_LP-21_F	CCGGAGCTGATATTGAAAGC	
mpx_LP-22_R	CGGTTCTTTCAAGTTCTTTTATGG	
mpx_cDNA_F	GGATTGTCTGCTCCTCAGA	Amplify *mpx* exon12/13 junction from cDNA template
mpx_cDNA_R	CTTTCCAAGGCTCGAGAT	
csf3r_MO	GAAGCACAAGCGAGACGGATGCCAT	Antisense ATG morpholino oligonucleotide
spi1_MO	GATATACTGATACTCCATTGGTGGT	Antisense ATG morpholino oligonucleotide

Table S2. Computationally-derived custom parameters used to assess neutrophil migration following wounding

Parameter[1]	**Definition**
In-wound neutrophil number	Absolute number of neutrophils that reach the artificial region
In-wound neutrophil proportion	Ratio of "number of neutrophils that reach the artificial region" to the "total number of neutrophils"
Forward Ratio	Ratio of "displacements with effective velocity larger than 0.6" to the "total number of displacements"
Inside wound ratio	Ratio of "number of displacements inside the wound area" relative to "all the displacements"
Inside wound ratio 2	Ratio of "number of displacements inside the wound area" relative to "all the displacements after a neutrophil reached the wound region"
Idle wound ratio	Ratio of "number of displacements with absolute velocity lower than a certain level" relative to "all displacements inside the wound region"
Backward ratio	Ratio of "number of displacements with effective velocity larger than -0.6" to the "total number of displacements"
*Move away from wound ratio	Ratio of "number of displacements which are moving away from the wound with a oriented velocity larger than a given threshold after they have crossed the artificial boundary" relative to "those displacements with an absolute velocity larger than the same threshold after they have reached the wound" i.e. of the neutrophils that cross the boundary and remain active, this parameter shows how many turn back from the wound
Velocity	Average of absolute velocity per track
Oriented velocity	Average of oriented velocity per Track
Lateral velocity	Average of lateral velocity per track
Transiting wound neutrophil number	Number of tracks that enter the wound and leave
Transiting wound neutrophil ratio	Ratio of "tracks that enter the wound and leave" to "total number of tracks"
Delayed activation	Distance (μm) from edge of tail + time (s) after which the neutrophil became active in terms of rapid movement towards the wound
Normalized delayed activation	Delayed activation, where distance and time were normalized to adimensional values in the range of [0-0.5] each to have a total range of [0-1]

FOOTNOTES

1. The parameters were derived from the following computational methodologies (provided here in more detail than in Methods):

   The fluorescently-labeled neutrophils were tracked with a model-based tracking algorithm (Reyes-Aldasoro et al., 2009) adapted from the keyhole tracking algorithm presented in (Reyes-Aldasoro et al., 2008). The algorithm consisted of the following steps.

   (1) *Pre-processing,* which transformed the data into a sequence of binary images that contained segmented foreground objects (neutrophils). The computational complexity (number of operations and time required to process) was reduced by levels with a Gaussian Pyramid (Burt and Adelson, 1983). For each level, groups of 4 contiguous voxels were averaged and their mean value assigned to a new pixel thus halving the rows and columns dimensions. One levels of the pyramid reduced the data from 512 × 512 × 10 to 256 × 256 × 10 voxels. Besides reducing the dimensions, a smoothing effect was produced and noise was reduced. The intensities of each frame were thresholded with a hysteresis threshold as follows: voxels below a lower threshold were classified as background, and those above a higher threshold were classified as neutrophils. The remaining voxels between these two levels were then classified as neutrophils if they were in contact with voxels above the high threshold, or as background if otherwise. Both thresholds were automatically determined using Otsu's algorithm (Otsu, 1979), first on the reduced data for the high level and the logarithm of the data for the lower level. Once the neutrophils had been segmented, they were individually labeled. Finally, the centroids of each segmented neutrophils were determined, together with the distances that separated them from neighbors, if any.

   (2) *Tracking,* which linked the objects in contiguous frames to form the tracks by means of a keyhole model, which predicted the most probable landing position of a neutrophil at time *t+1* from the position in times *t-1* and *t*. The most probable step for a neutrophil that is moving from frame *t-1* to frame *t*, is to follow the direction of the previous steps with the same velocity to frame *t+1*. Assuming that a child neutrophil would move with the same direction and velocity as its parent, its landing position can be predicted. Of course, this would not cover changes in speed or turns. Two regions of probability where the neutrophil is most likely to land were therefore defined: a narrow wedge (60° wide) oriented towards the predicted landing position, and a truncated circle (300°) that complements the wedge; together they resemble a keyhole. Once all segmented neutrophils had been examined for possible parent-child relationships, a reduced number of them formed a series of tracks of different lengths.

(3) *Post-processing,* which removed links in tracks that could have resulted from noise, and joined sections that were considered to be split sections from a single track. The same keyhole model was used analyzing the movement backwards. That is, the same keyhole model used child (*t+1*) and grandchild (*t+2*) to generate a keyhole at time (*t*). If the neutrophil of a previous time point was found to land inside the keyhole, it remained as part of the track, otherwise it was removed. Finally outliers were removed: those tracks whose average velocity exceeded 3 times the standard deviation from the mean average velocity of the whole distribution were discarded together with tracks of 3 or less hops. One hop was a link between consecutive frames, thus only objects that were tracked between 5 or more frames were considered. In some cases, as neutrophils moved next to each other, they were too close to be distinguishable by the segmentation algorithm. In this case, the algorithm recorded which neutrophils formed the merger, together with their volumes. These data were later used to identify the individual objects, if the merged neutrophil split into two. For this dataset, it remains possible that broken tracks were a source of error, and account for some inconsistencies in the outcomes of comparisons for parameters based on displacements *vs* similar parameters based on tracks.

The tracking algorithm produced a series of 4D vectors [row × column × slice × time] for each neutrophil. To analyze the directionality of the movement and its nature (fast / slow, uniform / varying speed, direct / meandering etc.) a series of measurements based on the tracks were developed. In addition, approaches were developed to investigate if the neutrophils would reach the edge of the tail and stay, or move away. For this purpose, an artificial wound region was drawn next to the edge and parameters developed based on this region and the movement of the neutrophils in relation to it. The parameters summarized the behavior of each cell and/or the whole population of neutrophils per zebrafish.

Figure 6B shows an example of a 3-dimensional plot with rows and columns in the *x,y* axis with time as the *z*-axis, with the color of the tracks denoting the velocity of each object: dark blue and cyan corresponds to slow, red-brown to fast moving objects and green-yellow to intermediate ones. The DIC image of the fish is presented as a horizontal plane at time 0. Such a plot displays the kinetic behavior of the neutrophils. Firstly, it displays the general direction of movement of the cells, in this case from left to right. Secondly, the individual velocity is related to the slope of the lines, horizontal lines correspond to fast moving cells and vertical ones, to slow or nearly stationary cells. Thirdly, it displays how some cells migrate towards the wound, and once there, remain static. To investigate the movement further, a rotation of the axis was used to observe the movement towards the wound as one coordinate axis (*x*) and lateral movements as the other axis (*y*). Each movement could be analyzed as a vectorial projection, where the absolute velocity would correspond to the hypotenuse of a triangle where one cathetus corresponds to the oriented movement (towards the wound or backwards) and the other to the lateral movement. The oriented movements can be further analyzed in

terms of how effective they are in moving towards the wound: assigning +1 for movement parallel to the main orientation towards the wound, 0 for movement perpendicular to the main orientation, and -1 for perpendicular moving away from the wound, and between (-1,+1) for any other orientation. In this way, not only the absolute velocity (how fast the cell moved), but the oriented velocity (how fast it moved towards the wound), effective movements (ratio of displacements between frames that move more than a particular threshold) and other measurements could be observed.

From these tracks, the table above lists the exploratory measurements investigated. As an example, visual representation of the parameter asterisked in the table ("Move away from wound ratio") is found in Fig. 5A.

REFERENCES

Burt, P.J., and E.H. Adelson. 1983. The Laplacian Pyramid as a compact Image Code. *IEEE Trans. on Commun.* 31:532–540.

Otsu, N. 1979. A Threshold selection method from gray level histograms. *IEEE Trans. Syst. Man Cybern.* 9:62-66.

Reyes-Aldasoro, C.C., S. Akerman, and G.M. Tozer. 2008. Measuring the velocity of fluorescently labelled red blood cells with a keyhole tracking algorithm. *J Microsc* 229:162-173.

Reyes-Aldasoro, C.C., Y. Zhao, D. Coca, S.A. Billings, V. Kadirkamanathan, G.M. Tozer, and S.A. Renshaw. 2009. Analysis of immune cell function using in vivo cell shape analysis and tracking. In 4th IAPR International Conference on Pattern Recognition in Bioinformatics. V. Kadirkamanathan, editor Sheffield, UK.

Table S3. Overlap of leukocyte marker transgene expression in compound transgenic zebrafish embryos

Compound genotype	Age dpf	Number of cells (% of total)				Total number of cells
		Single transgene expression			Double transgene expression	
		lyz:DsRED2	*mpx*:EGFP	*mpeg1*:Kaede*		
lyz:DsRED2/ *mpx*:EGFP	2	16 (17%)	2 (2%)	na	78 (81%)	96
	3	12 (9%)	0	na	128 (91%)	140
	4	9 (5%)	0	na	160 (95%)	169
	3-WM¶	10 (7%)	0	na	125 (93%)	135
lyz:DsRED2/ *mpeg1*:Kaede	3	83 (59%)	na	58 (41%)	0	141

* Actual genotype Tg(*mpeg1*:GAL4)x(10xUAS:Kaede)
na = not applicable
¶ = Wound margin (WM) corresponds to cell within 100 μm of the wound edge 2 h after amputation.

SUPPLEMENTAL DATA FIGURE LEGENDS

Figure S1.

Hematopoietic gene expression in the *myeloperoxidase*-deficient zebrafish mutant *durif*, related to Fig. 1.

A-P. Gene expression by whole mount in situ hybridization in wildtype (WT) and *durif* (*drf*) embryos at the ages indicated. *drf* embryos result from homozygote incrossing. All views are direct lateral views except B,D,F,H which are ventral views corresponding to the panels to their left. *drf* shows normal expression of all these genes at the ages indicated.

Figure S2.

Injury-induced hydrogen peroxide levels are maintained for up to 3 h after injury in myeloperoxidase-deficient larvae, related to Figs 2 and 4.

A. Distributions of (i) the time of individual neutrophil arrival and (ii) the number of arriving and/or present neutrophils per embryo for all individual neutrophils in the embryos contributing to Figs 2B and 4A data, showing no significant difference between genotypes. Two-tailed Mann-Whitney test.

B. Percentage of maximum hydrogen peroxide levels at the wound zone for wildtype (blue) or *durif* (*drf*, red) 3-3.5 dpf zebrafish larvae. Curves show ratiometric 500/420 nm HyPer emission data from the wound zone region (~50 μm) for 360X 30 s time points collected

over 180 min on a Zeiss LSM 5 line scanning confocal microscope, normalised at percent of maximum. Curves in (i) are means for n = 5 (WT) and n=4 (*drf*). (ii) shows the individual median HyPer ratio profiles and corresponding p-values from a permutation test (see Methods). All scans on this instrument were independently scanned embryos, collected on 3 independent days. Data are exemplified in supplemental Movie M3.

C. Distributions of the time of individual neutrophil arrival (i) and the number of arriving and/or present neutrophils per embryo (ii) for all individual neutrophils and embryos contributing to the data in Fig. S2B. Two-tailed Mann-Whitney test.

Figure S3.

A single neutrophil is sufficient to reduce local wound zone H_2O_2 concentration.

A. Still images over 1 h showing path of a single *lyz*:DsRED2-marked neutrophil (upper row) and associated HyPer ratiometic data reflecting the H_20_2 concentration data for the wound zone. Note the asymmetrical regional reduction on the dorsal (upper) half of the fin where the DsRED2-marked neutrophil is located, most evident by the loss of extent of yellow signal on the heat map. Stills are from supplemental Movie M4**.** Scale bar, 100 μm.

B. Merged transmission and red fluorescence image at 98 min after injury, overlayed with the migratory paths of *lyz*:DsRED2 neutrophils (4 green paths, only one of which is relevant to regions 1 and 2) and

lyz:DsRED2-negative macrophages (purple, blue and cyan paths, all relevant to region 3). Regions 1-4 are: (1) and (2) regions where the single DsRED2-marked neutrophil passes in sequence; (3) region where 3 DsRED-2-negative macrophages pass; (4) control region, distal to wound. Scale bar, 100 μm.

C. HyPer ratiometic data reflecting the temporal H_20_2 concentration data for the 4 regions of the injured zebrafish larvae detailed in (B); data are median HyPer ratio for each of the regions shown. Note that the median H_20_2 concentration decreases in sequence in regions 1 then 2 as the neutrophil passes through them, but remains elevated in region 3 where only macrophages pass. The concentration of H_20_2 remains at background in the control region (4).

Figure S4.

Neutrophil numbers at a wound edge show consistent differences between wildtype and *myeloperoxidase*-deficient *durif* embryos, related to Fig. 6C.

Two additional independent experiments replicating the observations of Fig. 6C, showing consistent differences between wound edge neutrophil number profiles in wildtype (WT) and *durif* (*drf*) embryos.

A,B. The number of neutrophils (mean±SE) at the wound margin (within 80-100 μm of wound edge), for a larger wound involving the notochord, as shown in the schematic insert in Fig. 6C. Neutrophils

were marked by either the *mpx*:EGFP (A) or *lyz*:DsRED2 (B) transgene.

p-values for comparisons between groups at 4 and 6 h after injury: *=0.01, **0.0028, ***0.0001.

C. Tabulated descriptive and analytical statistics for data in Fig. 6C and (A) and (B) of this Supplementary figure.

na=not applicable, because the intercepts of the line cannot be tested for difference when the gradients of the lines being compared are not the same.

SUPPLEMENTAL DATA MOVIE LEGENDS

Movie M1.

Real time comparison of hydrogen peroxide concentrations in representative wildtype and leukocyte-depleted embryos after wounding, related to Fig. 2.

Video is a composite of 3 sets of 90 min time-lapse videomicroscopy data for 3 representative embryos: wildtype (WT, left), *spi1/csf3r* morphant (middle) and *cloche* (*clo*) mutant (right). Top row of panels are DIC images with *lyz*:DsRED2-positive neutrophils overlaid. Bottom row of panels show H_2O_2 concentrations represented as HyPer ratio heat map images (scale as in Fig. 2C). WT embryo displays a rapid increase in H_2O_2 concentration at the wound zone which declines to an intermediate level. In contrast, leukocyte-depleted *spi1/csf3r* morphant and *clo* embryo display a similar rapid

increase in H_2O_2 concentration at the wound which is maintained at a high level until the end of video at 90 min. Note the presence of a *lyz*:DsRED2-marked neutrophil adjacent to the circulation in *spi1/csf3r* morphant video. Images were acquired on a Nikon Ti-E microscope every minute for 83 min (8 min - 90 min after injury) (time stamp – bottom left). Note that due to bleed-through emission of DsRED2 into the $HyPer_{480}$ images, in the lower panel HyPer heatmap images, the signal in the small regions overlapping mobile DsRED2-marked neutrophils themselves is not a true indication of the H_2O_2 concentration at that site.

Movie M2.

Real time comparison of hydrogen peroxide concentration in representative wildtype and *myeloperoxidase*-deficient *durif* embryos after wounding, related to Fig. 4.

Video is a composite of 2 sets of 90 min time-lapse videomicroscopy data for 2 representative embryos: wildtype (WT, left), *myeloperoxidase*-deficient *durif* (*drf*) (right). Top row of panels are DIC images with *lyz*:DsRED2-positive neutrophils overlaid. Bottom row of panels show H_2O_2 concentrations represented as HyPer ratio heat map images (scale as in Fig. 1). WT embryo (left, same embryo as in supplemental Movie M1) displays a rapid increase in H_2O_2 concentration at the wound zone which declines to an intermediate level; during this period, 5 *lyz*:DsRED2-marked neutrophils arrive at the wound edge. In contrast, the *drf* embryo (right) displays a similar

rapid increase in H_2O_2 concentration which is sustained at high levels at the wound throughout the 90 minute period, even though 5 *lyz*:DsRED2–marked neutrophils have arrived at the wound edge. Note that this *drf* embryo demonstrates bursts of H_2O_2 production at small injuries (located in this embryo at 2 locations on ventral/lower edge of the fin), which wane with time. Images were acquired on a Nikon Ti-E microscope every minute for 83 min (8 min - 90 min after injury) (time stamp – bottom left).

Movie M3.

Real time comparison of hydrogen peroxide concentrations in wildtype and *myeloperoxidase*-deficient *durif* (*drf*) embryos for 3 h after wounding, related to Fig. S2B.

Video is a composite of 2 sets of 183 min time-lapse videomicroscopy data for 2 representative embryos: wildtype (WT, left), *myeloperoxidase*-deficient *durif* (*drf*) (right). Top row of panels are DIC images with *lyz*:DsRED2-positive neutrophils overlaid. Bottom row of panels show H_2O_2 concentrations represented as HyPer ratio heat map images (scale as in Fig. 2C). WT embryo (left) displays a rapid increase in [H_2O_2] at the wound zone which declines to an intermediate level; during this period, 10 *lyz*:DsRED2-marked neutrophils arrive at the wound edge, some of which exhibit peripatetic in-wound migration. In contrast, the *drf* embryo (right) displays a similar rapid increase in H_2O_2 concentration which is sustained at high levels at the wound throughout the 180 min period,

even though 4 *lyz*:DsRED2–marked neutrophils arrive at the wound edge. Note the delay in *drf* neutrophils initiating their migration to the wound edge, in comparison to the prompt migration of WT neutrophils. Images were acquired on a Zeiss LSM 5 Live line scanning confocal microscope every 30 sec for 3 hours (time stamp – bottom left).

Movie M4.

Changes in wound margin hydrogen peroxide concentration as a single *lyz*:DsRED2-marked neutrophil migrates to and within the wound zone, related to Fig. S3.

Video is one set of 90 min time-lapse videomicroscopy data. Left panel is a DIC image of the tail with *lyz*:DsRED2-positive neutrophils overlaid. Right panel shows the changes in H_2O_2 concentrations represented as HyPer ratio heat map images (scale as in Fig. 1). Note the migration of the single *lyz*:DsRED2-marked neutrophil to the dorsal/upper wound zone correlates with a greater decline in H_2O_2 concentration within that zone than in the ventral/lower zone. Furthermore, this is despite 3 non- *lyz*:DsRED2-marked leukocytes migrating to the ventral/lower zone, which are likely to be non-myeloperoxidase-expressing macrophages. For a more detailed description, explanation and analysis of this video, see Fig. S3 and the associated text. Images were acquired on a Nikon Ti-E microscope every minute for 90 min (time stamp – bottom left).

Supplemental Figure 1

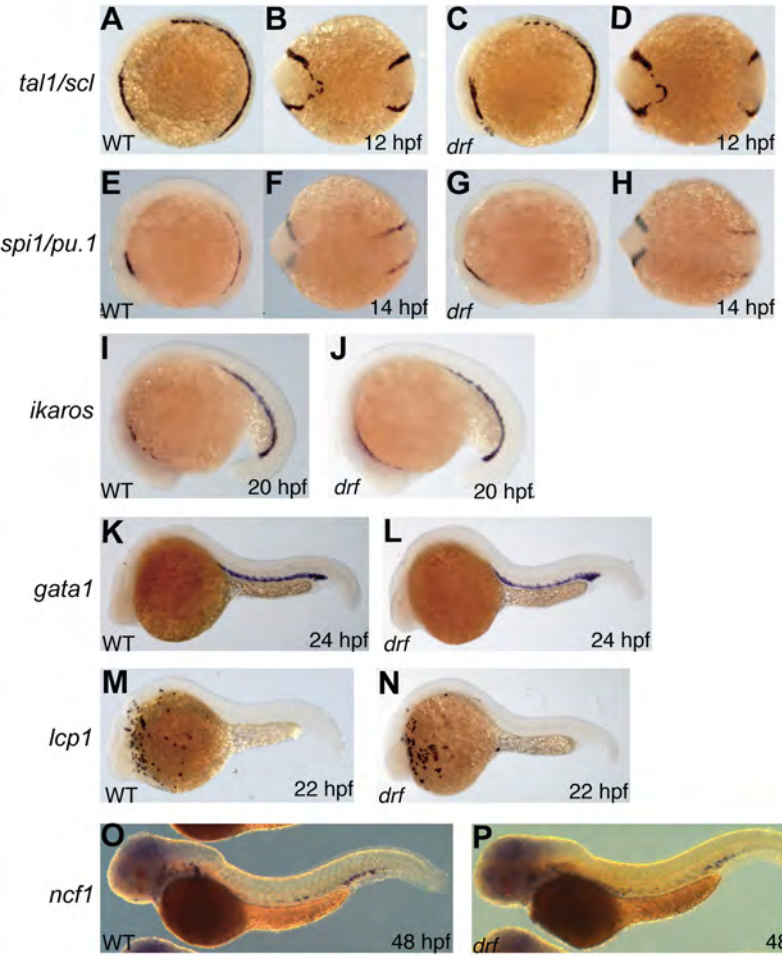

Supplemental Figure S2

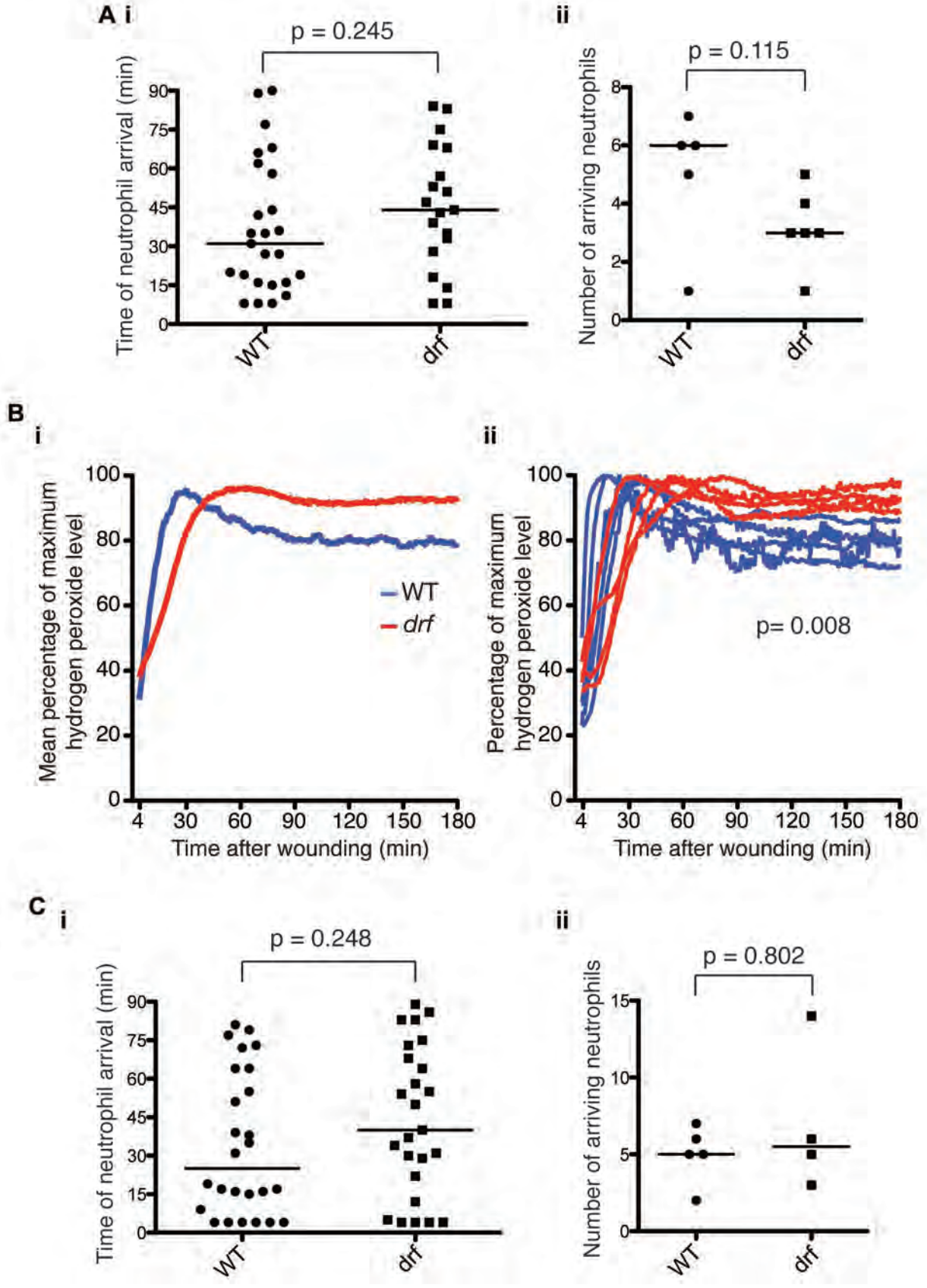

Supplemental Figure S3

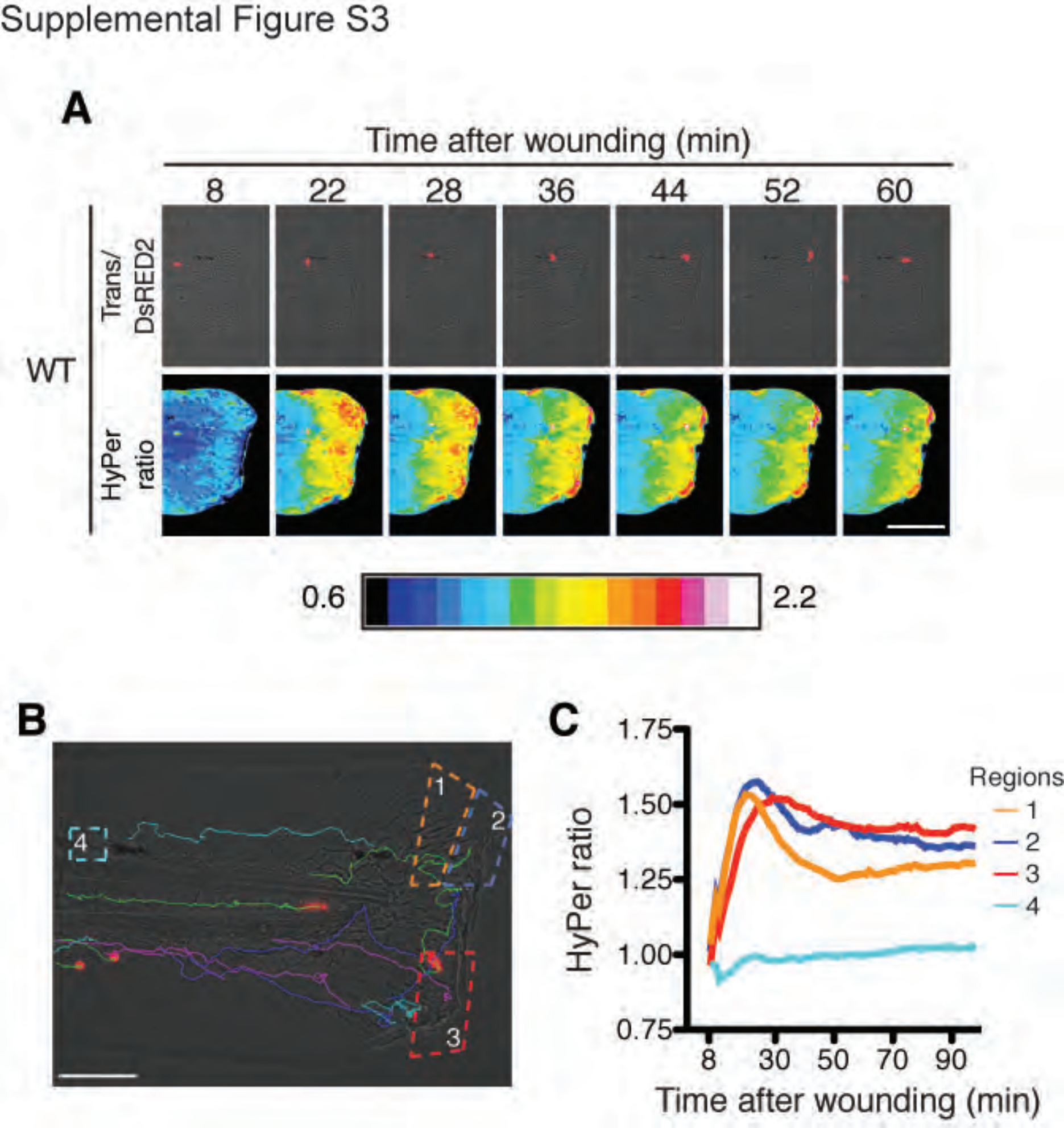

Supplemental Figure S4

A

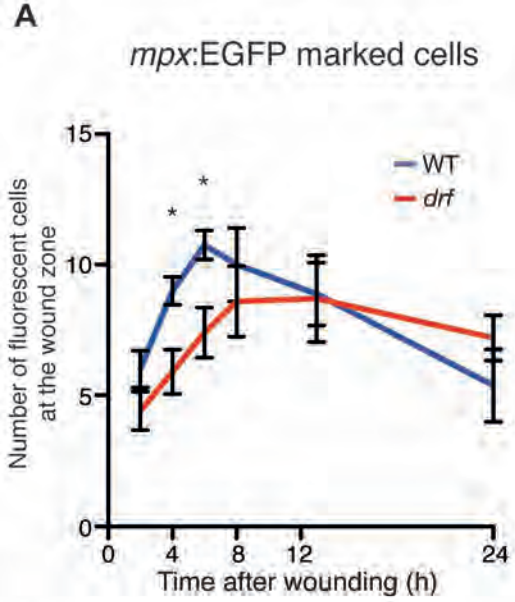

B

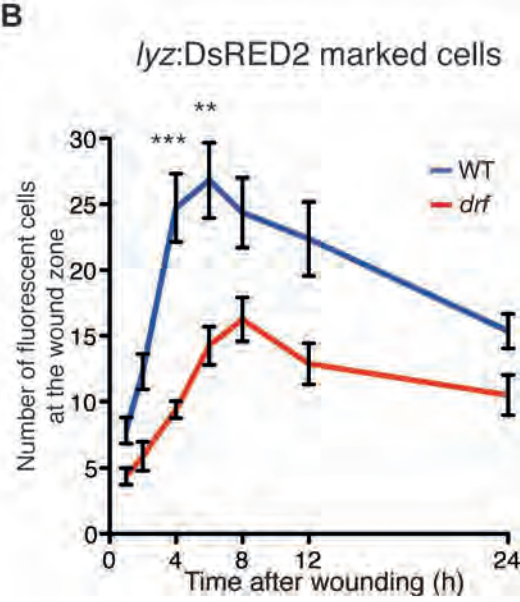

C

Data	Genotype	n	Time to peak hours after injury	Slope to peak neutrophils/hour	p value for slope gradient	p value for slope elevation
Fig. 6C	WT *mpx*:EGFP	12	1-6	3.23 ± 0.49	0.002	na
	drf mpx:EGFP	12	1-8	1.73 ± 0.20		
Supp Fig. 4A	WT *mpx*:EGFP	8	2-6	1.19 ± 0.21	0.21	0.0002
	drf mpx:EGFP	10	2-8	0.71 ± 0.22		
Supp Fig. 4B	WT *lyz*:DsRED2	11	1-6	4.03 ± 0.56	0.0001	na
	drf lyz:DsRED2	8	1-8	1.79 ± 0.20		